

1 Title

2 Cross-species functional diversity within the PIN auxin efflux protein family

3 Authors

4 Devin Lee O'Connor^{1,^}, Mon Mandy Hsia², John Vogel^{3,4}, Ottoline Leyser¹.

5 Affiliations

6 ¹Sainsbury Laboratory University of Cambridge, Cambridge, UK.

7 ²USDA-ARS Western Regional Research Center, Albany, CA.

8 ³U.S. Department of Energy Joint Genome Institute, Walnut Creek, CA.

9 ⁴Department of Plant and Microbial Biology, University of California, Berkeley, CA.

10 [^]Author for Correspondence: Devin Lee O'Connor devin.oconnor@slcu.cam.ac.uk

11

12 Abstract

13 In plants, directional transport of the hormone auxin creates auxin concentration
14 maxima and paths of transport that provide positional, polarity, and growth regulatory
15 cues throughout development. In *Arabidopsis thaliana*, the polar-localized auxin
16 transport protein PIN-FORMED1 (AtPIN1) is required to coordinate development
17 during flowering. However, Arabidopsis has a derived PIN family structure; the
18 majority of flowering plants have retained a clade of PIN proteins phylogenetically
19 sister to PIN1, the Sister-of-PIN1 clade (SoPIN1), which has been lost in the
20 Brassicaceae, including Arabidopsis. Based on PIN localization in the grasses
21 *Brachypodium distachyon* and *Zea mays*, which have both SoPIN1 and PIN1 clades,
22 we previously proposed that the organ initiation and vein patterning roles attributed to
23 AtPIN1 were shared between the SoPIN1 and PIN1 clades in grasses. Here we show
24 that *sopin1* and *pin1b* mutants have distinct phenotypes in *Brachypodium* and thus
25 the two clades are not functionally equivalent. *sopin1* mutants have severe organ
26 initiation defects similar to Arabidopsis *atpin1* mutants, while *pin1b* mutants initiate
27 organs normally but have increased stem elongation. Heterologous expression of
28 *Brachypodium* PIN1b and SoPIN1 in Arabidopsis *atpin1* mutants provides further
29 evidence for functional distinction between the two clades. SoPIN1 but not PIN1b can
30 complement null *atpin1* mutants, while both SoPIN1 and PIN1b can complement an
31 *atpin1* missense allele with a single amino acid change. The different localization
32 behaviors of SoPIN1 and PIN1b when heterologously expressed in Arabidopsis
33 provide insight into how PIN accumulation at the plasma membrane, tissue-level
34 protein accumulation, transport activity, and interaction, all contribute to the
35 polarization dynamics that distinguish PIN family members. Combined, these results
36 suggest that the PIN polarization and trafficking behaviors required for organ initiation
37 differ from those required for other PIN functions in the shoot, and that in most
38 flowering plants these functions are split between two PIN clades.

39 Introduction

40 The plant hormone auxin is an essential mobile signal controlling growth and
41 patterning throughout plant development (Leyser, 2010). Auxin can passively enter
42 cells, triggering a vast array of downstream signaling events (Wang and Estelle, 2014),
43 but it cannot easily exit the cell without active transport (Raven, 1975; Rubery and
44 Sheldrake, 1974). As a result, directional efflux mediated by the polar-localized PIN-
45 FORMED (PIN) efflux carriers can organize auxin accumulation patterns, creating
46 concentration maxima and paths of transport that regulate growth, position organs,
47 and pattern tissues (Adamowski and Friml, 2015). Because auxin itself feeds back to
48 regulate PIN-mediated transport both transcriptionally and post-transcriptionally
49 (Leyser, 2006), the transport system shows remarkable robustness and plasticity. For
50 example, within the PIN family compensatory changes in PIN abundance can mitigate
51 PIN loss-of-function mutant phenotypes (Blilou et al., 2005; Paponov et al., 2005;
52 Vieten et al., 2005), environmental inputs can trigger tissue-level changes in PIN
53 abundance and polarity leading to altered plant growth (Habets and Offringa, 2014),
54 and auxin transport paths can be reorganized in response to injury (Xu et al., 2006),
55 or spontaneously in tissue culture (Gordon et al., 2007). The self-organizing properties
56 of the auxin transport system thus gives this patterning mechanism extraordinary
57 versatility, and allows it to coordinate local and long range communication in the plant.

58 The correct initiation and positioning of organs (leaves, flowers, stems) in the growing
59 tip, or shoot apical meristem, of *Arabidopsis thaliana* (*Arabidopsis*) plants requires the
60 action of the PIN-FORMED1 (AtPIN1) auxin efflux carrier (Okada, 1991). AtPIN1 is
61 targeted to the plasma membrane and polarized in cells (Gälweiler et al., 1998). In the
62 meristem epidermis, polarization of AtPIN1 in neighboring cells converges around the
63 initiation sites of new organs, suggesting that polarized AtPIN1 concentrates auxin into
64 local maxima causing organ initiation (Benková et al., 2003; Heisler et al., 2005;
65 Reinhardt et al., 2003). Accordingly, in *atpin1* loss-of-function mutants, or if auxin
66 transport is pharmacologically inhibited, organ initiation is aborted, but it can be
67 rescued with local auxin application to the meristem flank (Reinhardt et al., 2003;
68 Reinhardt et al., 2000). Organ initiation in *atpin1* mutants can also be rescued with
69 epidermal-specific AtPIN1 expression (Bilsborough et al., 2011) and reducing AtPIN1
70 function specifically in the epidermis compromises organ positioning and initiation
71 (Kierzkowski et al., 2013), demonstrating the importance of convergent AtPIN1
72 polarization in the epidermis during organ formation.

73 The recurrent formation of AtPIN1 convergence points surrounding auxin maxima in
74 the meristem epidermis has been the focus of several computational models that
75 attempt to explain how auxin feeds back on its own transport via AtPIN1 to polarize
76 toward auxin maxima and control organ spacing (Abley et al., 2016; Bayer et al., 2009;
77 Jönsson et al., 2006; Smith, 2006; Stoma et al., 2008). However, AtPIN1 is also
78 expressed during the patterning of the vascular strands formed coincident with organ
79 positioning, and in these sub-epidermal cells AtPIN1 is polarized basally, away from
80 the presumed auxin maxima, suggesting that the control of AtPIN1 polarity with
81 respect to auxin is not consistent across tissues (Bayer et al., 2009).

82 Indeed, AtPIN1 is also expressed during patterning of leaf veins, and in mature tissues
83 (Gälweiler et al., 1998; Scarpella et al., 2006). During the vegetative phase, AtPIN1 is
84 not required for organ initiation but the organs that do form are misplaced and have
85 severe morphological and vascular defects, suggesting an important role for AtPIN1

86 in post-initiation morphogenesis and vein patterning in leaves, consistent with the
87 vascular patterning defects observed upon pharmacological inhibition of auxin
88 transport (Guenot et al., 2012; Sawchuk et al., 2013; Verna et al., 2015). Furthermore,
89 in mature tissues, AtPIN1 is expressed in vascular-associated cells and is required for
90 efficient long distance transport of auxin down the shoot in the polar auxin transport
91 stream, and this has been proposed to play an important role in the regulation of shoot
92 branching (Bennett et al., 2016; Bennett et al., 2006; Gälweiler et al., 1998; Shinohara
93 et al., 2013). Mutations in other PIN family members in combination with AtPIN1
94 mutants suggest further functions in embryo development, root development and
95 during plant growth responses to light and gravity (Leyser, 2005). Unfortunately, the
96 myriad roles for AtPIN1 during plant development are genetically obscured by the
97 severity of *atpin1* mutant organ initiation defects.

98 We previously showed that all sampled flowering plants outside of the Brassicacea
99 family have a clade of PIN proteins sister to the PIN1 clade (Sister-of-PIN1 or SoPIN1),
100 while Arabidopsis and other Brassicacea species have lost this clade (O'Connor et al.,
101 2014). During organ initiation in the grass *Brachypodium distachyon* (Brachypodium)
102 SoPIN1 is highly expressed in the epidermis, polarizes towards presumed auxin
103 maxima, and forms convergent polarization patterns during the formation of new
104 organs, suggesting a role in creating the auxin maxima required for organ initiation. In
105 contrast, the PIN1 clade members in Brachypodium, PIN1a and PIN1b, are not highly
106 expressed in the epidermis, orient away from presumed auxin maxima, and are
107 primarily expressed during patterning in the sub-epidermal tissues. Thus, the
108 combined expression domains and polarization behaviors of SoPIN1, PIN1a, and
109 PIN1b in Brachypodium largely recapitulate those observed for AtPIN1 in Arabidopsis.

110 The localization and polarization of the Brachypodium SoPIN1 and PIN1 clades can
111 be modeled with two different polarization modes with respect to auxin; SoPIN1
112 polarizes “up-the-gradient”, towards the neighboring cell with the highest auxin
113 concentration, while PIN1a and PIN1b polarize “with-the-flux”, accumulating in the
114 membrane with the highest auxin flux (O'Connor et al., 2014). Both polarization modes
115 were previously applied to AtPIN1 in order to capture the switch in polarity observed
116 during organ initiation and vein patterning, first orienting toward auxin maxima during
117 convergence point formation, then orienting away from maxima during vein patterning
118 below the epidermis (Bayer et al., 2009). These localization and modeling results
119 suggest that in most angiosperm species the organ placement and vascular patterning
120 functions attributed to AtPIN1 in *Arabidopsis* are split between the PIN1 and SoPIN1
121 clades, and that these two clades have different polarization properties with respect to
122 auxin.

123 Here we present the functional analysis of both SoPIN1 and PIN1 protein clade
124 members in Brachypodium, a species with the canonical two-clade family structure.
125 We show that SoPIN1 and PIN1b have different functions during Brachypodium
126 development, with SoPIN1 being required for organ initiation during the flowering
127 phase, and PIN1b regulating stem elongation. Using heterologous expression in
128 Arabidopsis, we show that the two proteins have different accumulation, polarization
129 and transport behaviors that result in different functional properties independent of
130 transcriptional context. These results suggest that the Arabidopsis AtPIN1 protein
131 represents an example of an evolutionary phenomenon the opposite of
132 subfunctionalisation in which protein functions are amalgamated into a single protein
133 rather than diversified amongst paralogs. AtPIN1 has a repertoire of roles, and

134 associated polarization behaviors that are distributed among several clades of PIN
135 proteins in most flowering plants.

136 **Results**

137 **SoPIN1 and PIN1b have different functions in Brachypodium**

138 During organ formation in the Brachypodium shoot, both SoPIN1 and PIN1b
139 expression precede PIN1a, which only accumulates significantly at the site of midvein
140 formation after the organ begins to grow. In the earliest stages of initiation, prior to the
141 periclinal cell divisions that are the hallmark of morphogenesis, SoPIN1 forms
142 convergent polarization patterns around the presumed auxin maxima in the meristem
143 epidermis, while PIN1b is expressed internally and orients away from the maxima
144 (O'Connor et al., 2014). Because of their early expression and opposing polarization
145 patterns, we focused on characterizing SoPIN1 and PIN1b as representatives of the
146 SoPIN1 and PIN1 clades.

147 As a first step towards understanding the functional differences between the SoPIN1
148 and PIN1 clades, we targeted Brachypodium SoPIN1 and PIN1b with CRISPR and
149 recovered loss-of-function mutants in both genes (see methods). Both *sopin1-1* and
150 *pin1b-1* mutants have single base-pair lesions that result in frame-shifts and
151 premature stop codons (Figure 1A). *sopin1-1* mutants show severe organ initiation
152 defects in the inflorescence remarkably similar to loss-of-function *atpin1* mutants in
153 *Arabidopsis* (Figure 1B-C, Figure 1 – supplement 1)(Okada, 1991). The indeterminate
154 flowering shoots of the Brachypodium inflorescence, called spikelets (Figure 1B,
155 inset), often fail to initiate in *sopin1-1* despite sometimes clear definition of node vs
156 internode tissue (n, and i, in Figure 1C). When spikelets do form, the spikelet
157 meristems are often devoid of new organs (Arrows in Figure 1C inset).

158 In wildtype spikelet meristems, SoPIN1 convergence point formation is coincident with
159 a decrease in the nuclear auxin response reporter protein DII-Venus (Brunoud et al.,
160 2012) (DII) (Figure 1E), which functions in Brachypodium and is degraded in the
161 presence of auxin in spikelets (Figure 1 - supplement 2). In *sopin1-1* meristems DII
162 accumulation is uniformly high for long stretches of the epidermis, and the patterned
163 reduction of DII both in the meristem epidermis and internally fails to occur, suggesting
164 a failure to organize auxin maxima (Figure 1F arrow).

165 In contrast to the severe defects of *sopin1-1*, organ initiation in *pin1b-1* mutants is
166 unaffected (Figure 1D). However, *pin1b-1* mutants show minor shoot twisting and
167 increased internode (stem tissue) length, especially in the basal few internodes
168 (Figure 1G, 1H). The longer internodes of *pin1b-1* lead to an overall increase in plant
169 height (Figure 1H). The internode defects of *pin1b-1* are consistent with the abundant
170 PIN1b expression observed in wildtype stem tissue (Figure 1I). The difference in
171 phenotypes between *sopin1-1* and *pin1b-1* Brachypodium mutants suggests a
172 functional distinction between the SoPIN1 and PIN1 clades, and reveals that while
173 PIN1b is expendable for organ initiation, it is involved in the regulation of internode
174 growth.

175

176 **SoPIN1 and PIN1b accumulate differently in Arabidopsis**

177 The difference in the *sopin1-1* and *pin1b-1* phenotypes in *Brachypodium* may be due
178 to their different expression patterns and not necessarily to differences in polarization
179 behavior as previously hypothesized (O'Connor et al., 2014). In order to explore what
180 functional differences exist between the proteins themselves, we expressed both
181 *Brachypodium* proteins in wildtype (Columbia, Col-0) *Arabidopsis* under the control of
182 a 3.5kb *Arabidopsis PIN1* promoter fragment known to drive PIN1 expression
183 sufficient to complement *pin1* mutants (*proAtPIN1*) (Heisler et al., 2005). Remarkably,
184 despite the loss of SoPIN1 from *Arabidopsis*, *Brachypodium* SoPIN1 created clear
185 convergent polarization patterns around the sites of organ initiation in inflorescence
186 meristems (Figure 2I asterisk, 25 of 27 meristems from 4 independent transgenic
187 events). SoPIN1 protein abundance was highest in the meristem epidermis and
188 SoPIN1 convergence points were most clearly observed surrounding I2 and I1
189 primordia (Figure 2A). Immediately below the apex, SoPIN1 accumulated in an ill-
190 defined ring shape within which the vascular bundles will form (Figure 2J, 15 of 23
191 meristems from 4 independent events).

192 In contrast, significant PIN1b accumulation was absent from the meristem epidermis
193 in 19 of 29 meristems from 7 independent transgenic events. In the few meristems
194 where PIN1b was significantly expressed in the epidermis, it did not show clear
195 convergent polarization patterns, and its polarity was often unclear (Figure 2B). Within
196 initiating organs PIN1b often localized to punctate vesicular bodies inside cells not the
197 cell membrane (Figure 2B arrow). The PIN1b expression level remained low just below
198 the meristem apex, but in contrast to SoPIN1, PIN1b formed defined domains around
199 the presumptive developing vascular bundles (Figure 2L). The lack of PIN1b protein
200 in the meristem epidermis was not due to silencing of the transgene in these lines
201 because we observed abundant PIN1b protein in the developing vasculature below
202 the apex, even in plants where the meristem had no epidermal expression (Figure 2D)
203 (8 samples from 4 events). In the same tissues SoPIN1 accumulated in both the
204 vasculature and the epidermis (Figure 2C) (5 samples from 2 events).

205 In order to determine whether there were also tissue-level differences in protein
206 accumulation in mature tissues, we imaged SoPIN1 and PIN1b in the basal internode.
207 Here, AtPIN1 normally accumulates in a highly polar manner in the root-ward plasma
208 membranes of cambium (c) and xylem parenchyma (xp) tissues of the vasculature
209 (Bennett et al., 2016; Gälweiler et al., 1998). PIN1b accumulated in a similar pattern
210 to AtPIN1 (Figure 2F, 2H. 10 samples from 5 independent transgenic events). In
211 contrast, in addition to accumulating in the cambium and xylem parenchyma, SoPIN1
212 accumulated in the central pith tissue (p) (Figure 2E, 2G. 15 samples from 4
213 independent transgenic events). AtPIN1 is not normally observed in the pith (Bennett
214 et al., 2016; Gälweiler et al., 1998). In the basal internode both proteins showed the
215 characteristic AtPIN1 root-ward polarization pattern regardless of tissue-level
216 abundance (Figure 2K, 2M).

217 Taken together, these results show that even under the same transcriptional control
218 SoPIN1 and PIN1b show distinct tissue-level accumulation patterns in *Arabidopsis*.
219 While the overall behavior of the two *Brachypodium* proteins is similar to AtPIN1 in
220 many tissues, there are behaviors unique to each *Brachypodium* PIN even under the
221 AtPIN1 promoter. PIN1b fails to accumulate in the epidermal tissues where AtPIN1
222 and SoPIN1 remain high, whereas SoPIN1 accumulates in the pith tissue where

223 AtPIN1 and PIN1b do not. The convergent polarization patterns of SoPIN1 and the
224 vascular accumulation of PIN1b in Arabidopsis are remarkably similar to their native
225 behaviors in *Brachypodium* (O'Connor et al., 2014).

226

227 **SoPIN1 but not PIN1b can restore organ initiation and bulk auxin** 228 **transport in AtPIN1 null mutants**

229 To determine whether the observed differences in SoPIN1 and PIN1b polarization and
230 accumulation have functional consequences in Arabidopsis, we used the *proAtPIN1*
231 driven SoPIN1 and PIN1b constructs to complement the Arabidopsis *pin1-613* mutant
232 (also known as *pin1-7*). The *pin1-613* allele is a putative null T-DNA insertion mutant
233 with severe organ initiation defects in the inflorescence (Bennett et al., 2006; Smith,
234 2006; Zourelidou et al., 2014). Given that epidermal PIN1 function is important for
235 organ initiation (Bilsborough et al., 2011; Kierzkowski et al., 2013), as expected only
236 SoPIN1 was able to complement the *pin1-613* mutation and mediate organ initiation
237 (Figure 3A) (3 out of 6 independent transgenic events showed complementation).
238 However, phenotypic complementation of *pin1-613* by SoPIN1 was incomplete, and
239 mature plants showed a variety of phenotypic defects (Figure 3A, Figure 3 -
240 supplement 1). Most notably, each flower produced more sepals and petals than wild-
241 type, but almost no stamens (Figure 3B, 3C, Figure 3 - supplement 2). SoPIN1
242 complemented *pin1-613* plants were thus sterile. We wondered if these phenotypes
243 could be explained if SoPIN1 had poor auxin transport function in Arabidopsis.
244 However, SoPIN1 restored wild-type levels of bulk auxin transport to *pin1-613* basal
245 internodes (Figure 3D). Thus SoPIN1 is at least in part functionally capable of initiating
246 organs and mediating root-ward auxin transport in the stem, but it is not functionally
247 identical to AtPIN1 under the same promoter.

248 In SoPIN1 complemented *pin1-613* mutants, SoPIN1 accumulation increased in the
249 meristem epidermis relative to wild-type or heterozygous plants, but the pronounced
250 convergent polarization patterns observed in the WT background were less clear
251 (Figure 4A, Figure 4 - supplement 1) (16 of 16 meristems). SoPIN1 complemented
252 meristems showed a variety of phyllotactic defects and had highly variable
253 morphologies (Figure 4 – supplement 1) (16 of 16 meristems). Similar to the pattern
254 observed in the wild-type background, sub-epidermal SoPIN1 in *pin1-613* mutants
255 accumulated in a loosely defined ring within which individual vein traces were difficult
256 to discern (Figure 4I) (13 of 16 meristems). In the mature tissues, SoPIN1 accumulated
257 in the epidermis, vasculature, and mature pith tissues similar to the wild-type
258 background (Figure 4C, 4E, 4G).

259 In contrast to SoPIN1, PIN1b-expressing *pin1-613* plants had pin-formed
260 inflorescences that were indistinguishable from *pin1-613* alone (Figure 3A) (all 7
261 events failed to complement). The lack of complementation mediated by PIN1b was
262 not caused by silencing or low expression level because abundant PIN1b signal was
263 observed in *pin1-613* meristems (23 of 26 *pin1-613* meristems from 7 independent
264 events). In most PIN1b expressing *pin1-613* samples, expression increased in the
265 epidermis relative to wildtype, forming a ring-shaped domain around the meristem
266 apex (Figure 4B, 4D arrow, Figure 4 - supplement 2) (14 of 19 meristem apices from
267 6 independent events). Unlike in the wildtype background, PIN1b in the epidermis of
268 *pin1-613* meristems was more consistently targeted to the membrane and polar

269 (Figure 4K). However, even with this elevated polar expression in the meristem
270 epidermis, PIN1b was unable to mediate organ initiation. Below the apex, PIN1b was
271 polarized root-ward in *pin1-613* meristems (Figure 4J), forming defined traces
272 associated with the vasculature (Figure 4F, 4L). In the basal stem of *pin1-613* mutants
273 PIN1b accumulated in a pattern similar to wild-type, although the arrangement of
274 vascular bundles was irregular (Figure 4H). Remarkably, despite clear polar PIN1b
275 expression in *pin1-613* mutant stems (Figure 4M), PIN1b was unable to rescue bulk
276 auxin transport in this tissue (Figure 3D).

277 Although PIN1b was incapable of supporting organ formation or mediating bulk
278 transport in *pin1-613*, when an auxin maximum was created artificially by addition of
279 lanolin paste infused with IAA, PIN1b epidermal accumulation increased during the
280 initiation of the resultant primordia (Figure 4 – supplement 3) (4 of 6 samples from 2
281 independent transgenic events). Thus, in the absence of AtPIN1, PIN1b accumulation
282 in the epidermis is still auxin responsive and capable polar localization in *pin1-613*
283 meristem epidermal tissue, but it is not able to mediate organ initiation itself. These
284 results demonstrate that when expressed in *Arabidopsis*, there is a clear functional
285 separation between SoPIN1 and PIN1b independent of transcriptional control.

286

287 **SoPIN1 and PIN1b show different behaviors when expressed in the** 288 **meristem epidermis**

289 Epidermal-specific AtPIN1 expression is sufficient to rescue organ initiation in *atpin1*
290 mutants (Bilsborough et al., 2011). In order to drive increased PIN1b expression in the
291 epidermis, and to help reduce transgene position-effect variation of expression level,
292 we utilized a two-component expression system in the Landsberg *erecta* (*Ler*)
293 background to drive SoPIN1 and PIN1b under the control of the epidermis-enriched
294 Arabidopsis ML1 promoter (Hereafter designated *proAtML1>>*) (Lenhard, 2003;
295 Sessions et al., 2002). Under the control of *proAtML1* we achieved consistently high
296 epidermal expression of both SoPIN1 and PIN1b, but similar to the *proAtPIN1* driven
297 localization described above, only SoPIN1 showed clear convergent polarization
298 patterns around the sites of organ initiation (Figure 5A-5D, Figure 5 supplement 1 and
299 2) (9 of 9 meristems). Despite consistently high epidermal expression with this system,
300 PIN1b polarity remained difficult to determine, and in many cells the abundance of
301 protein on the membrane remained low (Figure 5D) (10 of 10 meristems). Instead,
302 PIN1b accumulated in intracellular bodies, especially in the cells of the apical dome
303 and the central domain of initiating organs (Figure 5B, 5D arrow). PIN1b abundance
304 and polarity was highest at the boundaries of lateral organs (Figure 5 - supplement 2).
305 Thus SoPIN1 and PIN1b show consistent behaviors in the meristem epidermis when
306 expressed under either *proAtPIN1* or *proAtML1*. Despite increased PIN1b expression
307 under *proAtML1*, and a resulting increase in protein accumulation in the apex, PIN1b
308 was still unable to form convergent polarization patterns in wildtype plants.

309

310

311

312 **Both SoPIN1 and PIN1b can rescue the Arabidopsis *pin1-4* mutation**
313 **when expressed in the meristem epidermis**

314 In order to determine whether the increased PIN1b abundance in the meristem
315 epidermis achieved by the *proAtML1* two-component system had functional
316 consequences, we crossed these transgenes into *pin1-4*. The *pin1-4* allele is in the
317 Landsberg *erecta* background and has a single P579 to L amino acid change in the
318 second-to-last transmembrane domain of AtPIN1 (Bennett et al., 1995), but the
319 phenotype is similarly severe to *pin1-613* (Figure 6A). Remarkably, both SoPIN1 and
320 PIN1b driven by *proAtML1* were able to rescue the organ formation defects of *pin1-4*
321 (Figure 6A). In contrast to the SoPIN1-mediated complementation of *pin1-613*
322 described above, both SoPIN1 and PIN1b-complemented *pin1-4* plants made WT
323 flowers that produced seed (Figure 6 – supplement 1). In addition, both *proAtML1*
324 SoPIN1 and PIN1b expressing *pin1-4* lines were able to rescue bulk auxin transport
325 in the basal internode, although PIN1b was less effective than SoPIN1 (Figure 6B).
326 Compared to wildtype and SoPIN1-complemented plants, PIN1b-complemented *pin1-*
327 *4* plants showed a significant increase in stem diameter (Figure 6C). Thus while both
328 proteins can complement the *pin1-4* organ initiation phenotype, the SoPIN1 and PIN1b
329 complemented lines have differing auxin transport properties and different plant
330 morphologies, suggesting once again that SoPIN1 and PIN1b are not functionally
331 identical.

332 SoPIN1-complemented *pin1-4* meristems were slightly smaller than wildtype, and in
333 rare cases showed defects in phyllotaxy (Figure 5 – supplement 1), but the protein
334 localization was similar to the pattern observed in the WT background, with clear
335 convergent polarization around initiating organs (Figure 5E, 5G). In contrast,
336 compared to the WT background, PIN1b localization in *pin1-4* was dramatically altered
337 (Compare Figure 5B with Figure 5F). Most obvious was an increase in membrane
338 targeted PIN1b and a corresponding reduction in intracellular PIN1b (Figure 5H).
339 PIN1b polarity in the *pin1-4* background was more apparent than in wildtype, and
340 convergent polarization patterns clearly marked incipient organs (Figure 5H). PIN1b-
341 complemented meristems accumulated less PIN protein in the apical dome compared
342 to SoPIN1-complemented meristems, and the meristems were larger (Figure 5 –
343 supplement 2).

344 In the basal internode, both PINs had similar accumulation patterns in the outer few
345 cell layers (Figure 5I-J arrows), and both showed basal polarization in the epidermis
346 (Figure 5K-L arrows). Despite this expression domain being drastically different than
347 the wildtype vascular-associated pattern of AtPIN1 (Bennett et al., 2006; Gälweiler et
348 al., 1998), expression in these few cortex layers and epidermis was apparently
349 sufficient to drive wildtype levels of rootward bulk auxin transport in *pin1-4* (Figure 6B).

350

351

352

353

354

355 Discussion

356 SoPIN1 and PIN1b have different functions in Brachypodium

357 During spikelet development in Brachypodium SoPIN1 forms convergent polarization
358 patterns surrounding the sites of organ initiation and strong expression of the auxin
359 response reporter DR5 (O'Connor et al., 2014). We provide additional evidence here
360 that SoPIN1 polarizes towards sites of high auxin concentration by showing that a DII-
361 Venus minimum occurs at SoPIN1 convergence points. In *sopin1* mutants the
362 reduction of DII does not occur, suggesting that SoPIN1 functions to concentrate auxin
363 at epidermal maxima, and similar to *Arabidopsis*, this is required for organ initiation in
364 the inflorescence. The specificity of SoPIN1 for the outer tissues in Brachypodium
365 provides further support for the idea that maxima formation is necessary for organ
366 initiation, and that this is primarily mediated by convergent PIN in the meristem
367 epidermis (Jönsson et al., 2006; Kierzkowski et al., 2013; Smith, 2006).

368 SoPIN1 clade mutants have been reported in the legume *Medicago truncatula* and in
369 tomato (*Solanum lycopersicum*), and these mutants show pleiotropic phenotypes
370 involving phyllotaxy, organ initiation, inflorescence branching, leaf serrations, and leaf
371 compounding, but they do not form barren pin meristems (Martinez et al., 2016; Zhou
372 et al., 2011). These wider morphogenetic events also involve epidermal PIN
373 convergence points and associated auxin maxima, suggesting a general role for
374 SoPIN1 clade members in generating such maxima (Barkoulas et al., 2008;
375 Bilsborough et al., 2011). But the lack of barren pin-formed meristems in these mutants
376 may suggest that different species are variably dependent on SoPIN1-generated
377 maxima for organ initiation.

378 In contrast to *sopin1*, loss of PIN1b function has no clear organ initiation defects,
379 despite being expressed in developing organs (O'Connor et al., 2014). Given that
380 auxin drainage is thought necessary for proper organ size and placement (Deb et al.,
381 2015), the lack of an organ initiation phenotype in *pin1b* is surprising. However, it is
382 possible that PIN1a performs some of this function, and double mutants are needed
383 to address the redundancy of PIN1a and PIN1b during organ initiation.

384 The increased internode elongation in *pin1b* mutants provides new genetic tractability
385 to address how PINs regulate tissue growth in the shoot independent of organ
386 initiation. Grasses contain intercalary meristems, bands of indeterminate tissue
387 separated from the apical meristem that are responsible for internode growth after
388 organ initiation. PIN1b expression around this meristematic tissue (Figure 1I) suggests
389 that PIN1b may regulate growth by influencing auxin distribution in this meristem. This
390 is consistent with evidence that loss of the ABCB1 auxin exporter in maize results in
391 dwarfism associated with reduced activity of intercalary meristems (Knöllner et al.,
392 2010). How PIN1b alters auxin dynamics to control internode growth will be an
393 important direction for future research.

394 The properties that define PIN behavior and function

395 **Membrane accumulation.** Because of their differing phenotypes in Brachypodium,
396 we used heterologous expression of SoPIN1 and PIN1b in *Arabidopsis* to explore the
397 ways in which different PIN family members may have different properties post-
398 transcription (Summarized in Figure 7). When expressed in the meristem epidermis in

399 wild-type Arabidopsis, SoPIN1 is localized to the membrane in most cells while PIN1b
400 often accumulates internally (Compare Figure 5C and D). Thus, with the same
401 transcriptional control different PINs can vary in the degree to which, after protein
402 production, they accumulate at the plasma membrane. The differential membrane
403 targeting of PIN1b and SoPIN1 is a tissue-specific phenomenon however, because
404 unlike in the epidermis, in the basal internode both PINs accumulate at the plasma
405 membrane (Figure 2K, 2M). The regulation of PIN plasma membrane polar targeting
406 and endocytic recycling has been an important avenue for understanding PIN function
407 and general membrane protein biology (Luschnig and Vert, 2014). Our results provide
408 further evidence that at least some of the signals governing membrane accumulation
409 are inherent in, and vary between different PIN family members.

410 **Tissue accumulation.** Under the same transcriptional control SoPIN1 and PIN1b
411 show different tissue-level accumulation patterns in Arabidopsis. In wildtype plants
412 *proAtPIN1*-expressed PIN1b shows less overall accumulation in the epidermis
413 compared to SoPIN1 (Compare Figure 2C and 2D). The punctate PIN1b signal in the
414 meristem epidermis may be PIN1b protein being actively targeted for degradation as
415 has been shown for PIN2 in the root (Abas et al., 2006). In contrast, SoPIN1 is
416 abundant in the epidermis and accumulates in an expanded expression domain in the
417 sub-epidermal meristem tissues (Compare Figure 2J and 2L). Also, in the basal
418 internode SoPIN1 accumulates in the pith tissue where AtPIN1 and PIN1b do not
419 (Figure 2E, 2G). The presence of SoPIN1 in the pith is not easy to explain because
420 AtPIN1 shows no protein accumulation in this tissue. It is possible however that the
421 sub-epidermal SoPIN1 protein accumulation in the meristem persists into the mature
422 internode.

423 In Arabidopsis, endogenous PIN family members show a degree of cross-regulation
424 where loss-of-function mutations in one PIN family member result in ectopic
425 accumulation of a different PIN in a compensatory pattern (Blilou et al., 2005; Paponov
426 et al., 2005; Vieten et al., 2005). We observed similar behavior in the *pin1-613* null
427 background where SoPIN1 and PIN1b accumulation in the meristem epidermis was
428 increased in the absence of AtPIN1 (Figure 4 supplements 1 and 2). However, we did
429 not observe the same cross-regulation in the *pin1-4* background where SoPIN1 and
430 PIN1b tissue-level accumulation seemed similar between *pin1-4* mutant and wild-type
431 meristems (Figure 5 - supplements 1 and 2). These variable tissue-level abundances,
432 and PIN cross-regulation behaviors highlight the overall redundancy of some PIN
433 behaviors, and further demonstrate the importance of PIN post-transcriptional
434 regulation for controlling PIN abundance.

435 **Transport activity.** In Arabidopsis, phosphorylation of PINs by several different
436 families of protein kinases is necessary for efficient auxin transport (Barbosa et al.,
437 2014; Jia et al., 2016; Willige et al., 2013; Zourelidou et al., 2014). The necessity for
438 PIN activation by phosphorylation may explain the inability of PIN1b to mediate bulk
439 auxin transport in the basal stem of *pin1-613* plants despite being expressed,
440 accumulating at the membrane, and being polarized rootward in this tissue (Figure
441 4M). It is possible that in the *proAtPIN1* domain PIN1b does not interact with the
442 appropriate activating kinase, and it is thus inactive. Indeed, a partially un-
443 phosphorylatable form of AtPIN1 fails to complement fully the bulk auxin transport
444 defect of *pin1-613* mutants in the basal internode (Zourelidou et al., 2014). However,
445 when expressed using *proAtML1*, PIN1b expression in the outer tissue layers of the
446 basal internode appears sufficient to mediate bulk auxin transport in *pin1-4* (Figure

447 6B), suggesting that PIN1b activity may be tissue dependent, perhaps because of the
448 differing expression domains of activating kinases (Zourelidou et al., 2014). Indeed,
449 Arabidopsis PIN4 and PIN7 are present in the *proAtML1* domain (Bennett et al., 2016),
450 making it conceivable that these PINs are the normal targets of activating kinases in
451 this tissue. Regardless, the behavior of PIN1b in *pin1-613* Arabidopsis provides a clear
452 indication that even once a PIN has accumulated at the cell membrane in a tissue it
453 may not be active.

454 **Interaction.** A particularly striking result is the ability of PIN1b to form convergent
455 polarization patterns and mediate organ initiation in the *pin1-4* missense mutant
456 background when it is unable to do so in the null *pin1-613* background. The strong
457 influence of *pin1-4* on PIN1b membrane targeting and polarity in the meristem
458 epidermis (Compare Figures 6D and 6H) suggests that PIN1b may be cooperating
459 with a partially functional *pin1-4* protein and together they recapitulate the functions of
460 wildtype AtPIN1. The presence of some *pin1-4* function is supported by the result that
461 SoPIN1 complementation of the null *pin1-613* allele is partial and because of flower
462 defects the plants are sterile (Figure 3B, 3C), while complementation of *pin1-4* is
463 complete and flowers are phenotypically normal and set seed (Figure 6 - supplement
464 1). Consistent with these different complementation phenotypes, SoPIN1 convergent
465 patterns are more evident in the presence of *pin1-4* than they are in the null *pin1-613*
466 background (Compare 4A and 5E). If PIN1b is indeed inactive in null *pin1-613* mutants
467 as we hypothesized above, then it is possible *pin1-4* facilitates the interaction of PIN1b
468 with the appropriate activating kinase, and this allows PIN1b to perform organ
469 initiation. Alternatively, *pin1-4* may provide polarity information that PIN1b lacks, and
470 even though *pin1-4* is non-functional, it is able to target or stabilize PIN1b on the
471 appropriate membrane to mediate convergent polarization patterns and organ
472 initiation. However, *pin1-4* interaction with PIN1b cannot explain the ability of PIN1b
473 to rescue bulk transport in the basal internodes of *pin1-4* mutants, because the two
474 proteins presumably do not overlap in this tissue. In this case the necessary interaction
475 between PIN1b and *pin1-4* may be set up early during organ initiation, and protein
476 modifications propagated to the basal internode. Direct PIN interaction has so far
477 never been shown, but if one PIN type can convey polarity or activity information to
478 another through direct interaction this may be important for understanding auxin
479 transport in tissues where multiple PINs overlap, such as in the root meristem (Blilou
480 et al., 2005), or in *Brachypodium* where multiple PINs are present during organ
481 initiation in the shoot (O'Connor et al., 2014).

482 **Polarity.** We previously showed that the polarization dynamics of SoPIN1, PIN1a, and
483 PIN1b in *Brachypodium* could be modeled by assigning two different polarization
484 modes to the SoPIN1 and PIN1 clades (O'Connor et al., 2014). In the model, SoPIN1
485 orients toward the adjacent cell with the highest auxin concentration, thus transporting
486 auxin up the concentration gradient and providing a positive feedback to concentrate
487 auxin into local maxima. In contrast, in the model PIN1a and PIN1b proteins are
488 allocated in proportion to auxin flux, thus providing a positive feedback where flux
489 through the tissue is amplified by the allocation of PIN1a/b in the direction of that flux.
490 The assignment of two different polarization modes was previously used to describe
491 the behavior of AtPIN1 during organ placement and vein patterning utilizing an auxin-
492 concentration based switching mechanism between the up-the-gradient (UTG) and
493 with-the-flux (WTF) polarization modes (Bayer et al., 2009). However, it has also been
494 suggested that a flux-based mechanism alone can account for both convergence
495 points and vein patterning (Abley et al., 2016; Stoma et al., 2008).

496 There are still no known mechanisms for direct sensing of intercellular auxin gradients
497 or flux across membranes, but the *sopin1* and *pin1b* phenotypes in *Brachypodium* are
498 consistent with the different polarization modes. SoPIN1 is required for organ initiation
499 and the formation of auxin maxima in *Brachypodium*, which is primarily modeled using
500 UTG polarization (Bayer et al., 2009; Jönsson et al., 2006; Smith, 2006). On the other
501 hand, *pin1b* mutant plants do not show organ initiation defects, but rather only have
502 internode elongation defects, a tissue where WTF models have been used to explain
503 PIN dynamics and measured auxin transport kinetics during vein patterning and the
504 regulation of branch outgrowth (Bayer et al., 2009; Bennett et al., 2016; Mitchison,
505 1980; Mitchison et al., 1981; Prusinkiewicz et al., 2009).

506 In wild-type *Brachypodium* the SoPIN1 and PIN1b expression domains are almost
507 entirely mutually exclusive (O'Connor et al., 2014), making it possible that the
508 observed polarization differences between the two clades are due to expression
509 context and not functional differences between the proteins themselves. More
510 specifically, perhaps an UTG mechanism dominates the epidermis while a WTF
511 mechanism is utilized in the internal tissues, and different PINs interact equally with
512 these context-dependent mechanisms. Our heterologous expression studies do not
513 exclusively support context-dependent or protein-dependent mechanisms for SoPIN1
514 and PIN1b polarity. It is clear that alone, only SoPIN1 and AtPIN1 show the convergent
515 polarization patterns associated with UTG polarization, and alone only SoPIN1 and
516 AtPIN1 are thus able to mediate organ initiation, while PIN1b cannot. On the other
517 hand, all three PINs are capable of root-ward polarization in the basal internode tissue.
518 The results presented here do not demonstrate whether within a single cell PIN1b and
519 SoPIN1 would orient differently with respect to auxin as might be expected for the dual
520 polarization model (O'Connor et al., 2014). However such context-independent
521 polarization behavior was previously observed for PIN1 and PIN2 in the root where
522 both PINs can polarize in opposing directions within a single cell type when expressed
523 in the PIN2 domain (Kleine-Vehn et al., 2008; Wisniewska et al., 2006).

524 **Outlook**

525 In total, our *Brachypodium* mutant phenotypes and heterologous expression results
526 point to multiple levels at which PIN family members can be functionally distinct.
527 Differential membrane targeting, tissue level accumulation, transport activity, indirect
528 or direct interaction, and the resultant polarity may all contribute to the dynamics of
529 PIN action during plant development. In most flowering plants two PIN clades, SoPIN1
530 and PIN1, with differing properties post-transcription mediate auxin transport in the
531 shoot, but these properties are seemingly combined into AtPIN1 in *Arabidopsis* and
532 other Brassicaceae species. Because PIN1b is unable to mediate organ initiation while
533 AtPIN1 can, and these two PINs are both members of the same clade, AtPIN1 may
534 have gained the ability to form convergent polarization patterns and mediate organ
535 initiation after, or coincident with, the loss of the SoPIN1 clade. Indeed, when
536 comparing Brassicaceae PIN1 proteins against a broad sampling of other angiosperm
537 PIN1 proteins, the Brassicaceae PIN1 proteins have several divergent protein
538 domains (Figure 7 - supplement 1), suggesting possible neofunctionalization within
539 the Brassicaceae family. Alternatively, an expansion of the PIN3,4,7 clade is also
540 characteristic of Brassicaceae species (O'Connor et al., 2014), making it possible
541 duplicated members of this clade buffered the loss of SoPIN1. However, there is no
542 indication that PIN3,4,7 have a role in organ initiation in the inflorescence (Guenot et
543 al., 2012). Regardless, we believe the combination of SoPIN1 and PIN1

544 characteristics into AtPIN1 coincident with the loss of the SoPIN1 clade represents a
545 form of reverse-subfunctionalization, the combination of functions originally split
546 between homologs into a single protein after gene loss. It is not surprising that PINs
547 may be particularly amenable to this kind of functional evolution because, as described
548 above, there are several post-transcriptional regulatory steps that ultimately combine
549 to control PIN function in plants. The output of auxin transport is the sum of a vast
550 network of post-transcriptional interactions that all act to regulate auxin transport itself,
551 and this gives the system plasticity during development, and perhaps also over
552 evolutionary time.

553

554 **Materials and Methods**

555 ***sopin1-1* and *pin1b-1* creation with CRISPR**

556 SoPIN1 (Bradi4g26300) and PIN1b (Bradi3g59520) were targeted with CRISPR using
557 vectors developed for rice (Miao et al., 2013). CRISPR constructs were transformed
558 into *Brachypodium* inbred line Bd21-3 using previously published methods (Bragg et
559 al., 2015).

560 *sopin1-1* CRISPR

561 The SoPIN1 guide was AGGCTGTCGTACGAGGAGT. This guide was shorter than
562 the typical 20bp in an effort to provide greater target specificity for SoPIN1 (Fu et al.,
563 2014). In the T0 regenerated plants, 5 out of 9 independent transgenic events showed
564 severe organ initiation defects, and all 5 contained lesions in the SoPIN1 CRISPR
565 target site. Unfortunately, only one of the events with a T0 phenotype set seed. In the
566 T1 progeny of this event only those individuals that contained the CRISPR transgene
567 showed lesions in the SoPIN1 CRISPR target site, and these plants showed the
568 *sopin1* phenotype and thus failed to set seed, suggesting active editing by the SoPIN1
569 CRISPR transgene in this event.

570 Not all events showed such efficient editing however, and we identified an independent
571 T1 family where a C insertion in the SoPIN1 CRISPR target site co-segregated with
572 the barren inflorescence phenotype. We designated this allele, which causes a
573 premature stop codon before the end of the third exon codon 739 base pairs
574 downstream from the target site, *sopin1-1*. We backcrossed a heterozygous *sopin1-1*
575 plant to the Bd21-3 parental line and all F1 progeny (N=4) were wild type. In the F2
576 generation, the *sopin1-1* lesion co-segregated with the barren inflorescence
577 phenotype (N=60: 32 het, 18 homo, 10 wt). Amongst these plants, 16 did not have the
578 Cas9 transgene, and the barren inflorescence phenotype still co-segregated with the
579 *sopin1-1* lesion (N=16: 8 het, 3 homo, 5 wt). We crossed the T1 *sopin1-1* heterozygous
580 plant with a line homozygous for the SoPIN1-Citrine genomic reporter line (O'Connor
581 et al., 2014). In the F2 we identified families homozygous for *sopin1-1* but segregating
582 for the SoPIN1-Citrine transgene. Only individuals that lacked the SoPIN1-Citrine
583 transgene showed a *sopin1-1* phenotype, while those that contained the SoPIN1-
584 Citrine transgene made spikelets and set seed. This complementation was
585 independent of the presence of Cas9.

586

587 *pin1b-1* CRISPR

588 The PIN1b guide was AGGGCAAGTACCAGATCC. We identified a single plant from
589 the regenerating T0 PIN1b CRISPR population that had longer basal internodes and
590 twisted leaves. This plant was homozygous for an A deletion in the PIN1b CRISPR
591 target site causing a premature stop in the second exon 502 base pairs downstream,
592 here designated *pin1b-1*. All T1 progeny showed the *pin1b* phenotype and were
593 homozygous for the *pin1b-1* lesion. We backcrossed these T1 plants to Bd21-3 and
594 all F1 progeny had a wild-type phenotype (N=11). In the F2, the *pin1b* phenotype co-
595 segregated with the *pin1b-1* lesion (N= 215, 91 het, 39 homo, 26 wt). Amongst these
596 plants, 24 did not have the Cas9 transgene, and the *pin1b* phenotype co-segregated
597 perfectly with the *pin1b-1* lesion (N=24: 10 het, 6 homo, 8 wt).

598 Reporter Constructs

599 All constructs were cloned using Multi-site Gateway (Invitrogen). For pZmUbi::DII-
600 Venus, we first cloned the maize ubiquitin promoter into pDONR P4-P1R (Primer IDs
601 1-2 Table 1) and this was subsequently recombined with pDONR 221 containing
602 Arabidopsis DII and pDONR P2R-P3 containing VENUS-N7 (Brunoud et al., 2012)
603 into the Multi-site Gateway binary vector pH7m34GW (<http://gateway.psb.ugent.be/>).
604 This construct was then transformed into Brachypodium Bd21-3 using previously
605 published methods (Bragg et al., 2015). In the T3 generation, degradation of DII-Venus
606 in the presence of auxin was validated by treating excised Brachypodium spikelet
607 meristems with 1 μ M 1-naphthaleneacetic acid (NAA) or mock treatment in 70%
608 ethanol, and imaging every 30 min (Figure 1 – figure supplement 2).

609 For *proAtPIN1* complementation, a 3.5kb Arabidopsis PIN1 promoter region was
610 amplified from a genomic clone previously reported to complement the *pin1* (Heisler
611 et al., 2005) and cloned into Gateway vector pDONR P4-P1R (Primer IDs 3-4 Table
612 1). For each Brachypodium PIN-Citrine fusion construct the entire coding region,
613 including the Citrine insertion, was amplified from the previously published reporter
614 constructs (O'Connor et al., 2014) and cloned into pENTR /D-TOPO (Primer IDs 5-8
615 Table 1). The *proAtPIN1* pDONR P4-P1R and PIN coding region vectors were then
616 recombined into Gateway binary vector pH7m24GW (<http://gateway.psb.ugent.be/>)
617 and transformed by floral dip into both Col-0 and plants heterozygous for *pin1-613*
618 (also known as *pin1-7*, SALK_047613) (Bennett et al., 2006; Smith, 2006).
619 Complementation was assessed in the T3 generation, and all plants were genotyped
620 for both the *pin1-613* mutation (Primer IDs 9-11 Table 1) and for presence of the PIN
621 transgene (Primer IDs 12-14 Table 1).

622 For the *proAtML1* lines the PIN coding regions with Citrine insertion pENTR /D-TOPO
623 Gateway vectors were recombined downstream of the two-component OP promoter
624 in vector pMoA34-OP (Moore et al., 1998) and then transformed into the *proAtML1*
625 driver line in the Landsberg *erecta* background (Lenhard, 2003). Lines homozygous
626 for both the *proAtML1* driver and OP::PIN were crossed to het *pin1-4* and
627 complementation was assessed in the F2 and F3 generations. All complemented
628 plants were genotyped for *pin1-4* (Primer IDs 15-16 Table 1 with Acil digestion), the
629 Brachypodium PINs (Primer IDs 12-14 Table 1), and the presence of the ML1 driver
630 transgene (Primer IDs 17-18 Table 1).

631

632 **Confocal Imaging**

633 All confocal images were captured on a Zeiss 780 laser scanning confocal using
634 514nm excitation. Detection wavelengths: 517-570nm for Citrine tagged PINs, 631-
635 717nm for Propidium Iodide, and 646-726 for chlorophyll A auto-fluorescence. The
636 pinhole was set to 1 airy unit for all meristem stacks and details of sub-epidermal
637 polarization, but was open to the maximum setting for tiled longitudinal and cross
638 sections of the basal internode (Figures 2C-H, 4C-H and 5I-J). Detection gain and
639 laser power were varied according to signal strength unless direct comparisons
640 between genotypes were made as indicated in figure legends.

641 **Auxin Transport Assays**

642 Auxin transport assays were carried out as described in (Crawford et al., 2010). Briefly,
643 17 mm long basal internodes were excised and the apical end submerged in 30 μ l
644 Arabidopsis salts (ATS) without sucrose (pH = 5.6) containing 1 μ M 14 C-IAA (American
645 Radiolabeled Chemicals). After 6 hours incubation, the basal 5 mm segment was
646 excised, cut in half, and shaken overnight at 400 RPM in 200 μ l scintillation liquid prior
647 to scintillation counting. 10 μ M N-1-Naphthylphthalamic Acid (NPA), an auxin transport
648 inhibitor, was added prior to incubation for negative controls.

649

650 **Acknowledgments**

651 Thanks to Fabrizio Ticchiarelli for genotyping help, Martin van Rongen for assistance
652 with transport assays and *pin1-613* oligos, Tom Bennett for *proAtPIN1* oligos, Marcus
653 Heisler for AtPIN1-GFP construct and *pin1-4* genotyping assistance, Teva Vernoux
654 for DII plasmids, and to all the members of the Leyser lab. Thanks also to Graeme
655 Mitchison and Katie Abley for helpful comments on the manuscript.

656

657 **References**

658 **Abas, L., Benjamins, R., Malenica, N., Paciorek, T., Wisniewska, J.,**
659 **Wirniewska, J., Moulinier-Anzola, J. C., Sieberer, T., Friml, J. and**
660 **Luschnig, C. (2006).** Intracellular trafficking and proteolysis of the
661 Arabidopsis auxin-efflux facilitator PIN2 are involved in root gravitropism.
662 *Nat Cell Biol* **8**, 249–256.

663 **Abley, K., Marée, A. F. and Coen, E. (2016).** Formation of polarity
664 convergences underlying shoot outgrowths. *eLife* **5**, 2061.

665 **Adamowski, M. and Friml, J. (2015).** PIN-Dependent Auxin Transport: Action,
666 Regulation, and Evolution. *The Plant Cell* **27**, 20–32.

667 **Barbosa, I. C. R., Zourelidou, M., Willige, B. C., Weller, B. and**
668 **Schwechheimer, C. (2014).** D6 PROTEIN KINASE activates auxin
669 transport-dependent growth and PIN-FORMED phosphorylation at the

- 670 plasma membrane. *Dev Cell* **29**, 674–685.
- 671 **Barkoulas, M., Hay, A., Kougioumoutzi, E. and Tsiantis, M.** (2008). A
672 developmental framework for dissected leaf formation in the Arabidopsis
673 relative *Cardamine hirsuta*. *Nat Genet* **40**, 1136–1141.
- 674 **Bayer, E. M., Bayer, E. M., Smith, R. S., Mandel, T., Nakayama, N., Sauer,**
675 **M., Prusinkiewicz, P. and Kuhlemeier, C.** (2009). Integration of transport-
676 based models for phyllotaxis and midvein formation. *Genes Dev* **23**, 373–
677 384.
- 678 **Benková, E., Michniewicz, M., Sauer, M., Teichmann, T., Seifertová, D.,**
679 **Jürgens, G. and Friml, J.** (2003). Local, Efflux-Dependent Auxin Gradients
680 as a Common Module for Plant Organ Formation. *Cell* **115**, 591–602.
- 681 **Bennett, S. R. M., Alvarez, J., Bossinger, G. and Smyth, D. R.** (1995).
682 Morphogenesis in pinoid mutants of *Arabidopsis thaliana*. *Plant J* **8**, 505–
683 520.
- 684 **Bennett, T. A., Hines, G., van Rongen, M., Waldie, T., Sawchuk, M. G.,**
685 **Scarpella, E., Ljung, K. and Leyser, H. M. O.** (2016). Connective Auxin
686 Transport in the Shoot Facilitates Communication between Shoot Apices.
687 *PLoS Biol* **14**, e1002446.
- 688 **Bennett, T. A., Sieberer, T., Willett, B., Booker, J., Luschnig, C. and Leyser,**
689 **H. M. O.** (2006). The Arabidopsis MAX Pathway Controls Shoot Branching
690 by Regulating Auxin Transport. *Current Biology* **16**, 553–563.
- 691 **Bilsborough, G. D., Runions, A., Barkoulas, M., Jenkins, H. W., Hasson,**
692 **A., Galinha, C., Laufs, P., Hay, A., Prusinkiewicz, P. and Tsiantis, M.**
693 (2011). Model for the regulation of *Arabidopsis thaliana* leaf margin
694 development. *Proc Natl Acad Sci USA* **108**, 3424–3429.
- 695 **Blilou, I., Xu, J., Wildwater, M., Willemsen, V., Paponov, I., Friml, J.,**
696 **Heidstra, R., Aida, M., Palme, K. and Scheres, B.** (2005). The PIN auxin
697 efflux facilitator network controls growth and patterning in *Arabidopsis* roots.
698 *Nature* **433**, 39–44.
- 699 **Bragg, J. N., Anderton, A., Nieu, R. and Vogel, J. P.** (2015). Brachypodium
700 *distachyon*. *Methods Mol Biol* **1223**, 17–33.
- 701 **Brunoud, G., Wells, D. M., Oliva, M., Larrieu, A., Mirabet, V., Burrow, A. H.,**
702 **Beeckman, T., Kepinski, S., Traas, J., Bennett, M. J., et al.** (2012). A
703 novel sensor to map auxin response and distribution at high spatio-temporal
704 resolution. *Nature* **482**, 103–106.
- 705 **Crawford, S., Shinohara, N., Sieberer, T., Williamson, L., George, G.,**
706 **Hepworth, J., Muller, D., Domagalska, M. A. and Leyser, H. M. O.** (2010).

- 707 Strigolactones enhance competition between shoot branches by dampening
708 auxin transport. *Development* **137**, 2905–2913.
- 709 **Deb, Y., Marti, D., Frenz, M., Kuhlemeier, C. and Reinhardt, D.** (2015).
710 Phyllotaxis involves auxin drainage through leaf primordia. *Development*
711 **142**, dev.121244–2001.
- 712 **Fu, Y., Sander, J. D., Reyon, D., Cascio, V. M. and Joung, J. K.** (2014).
713 Improving CRISPR-Cas nuclease specificity using truncated guide RNAs.
714 *Nat Biotechnol* **32**, 279–284.
- 715 **Gälweiler, L., Guan, C., Müller, A., Wisman, E., Mendgen, K., Yephremov,**
716 **A. and Palme, K.** (1998). Regulation of Polar Auxin Transport by AtPIN1 in
717 Arabidopsis Vascular Tissue. *Science* **282**, 2226–2230.
- 718 **Gordon, S. P., Heisler, M. G., Reddy, G. V., Ohno, C., Das, P. and**
719 **Meyerowitz, E. M.** (2007). Pattern formation during de novo assembly of
720 the Arabidopsis shoot meristem. *Development* **134**, 3539–3548.
- 721 **Guenot, B., Bayer, E. M., Bayer, E., Kierzkowski, D., Smith, R. S., Mandel,**
722 **T., Zádňíková, P., Benková, E. and Kuhlemeier, C.** (2012). Pin1-
723 independent leaf initiation in Arabidopsis. *Plant Physiol* **159**, 1501–1510.
- 724 **Habets, M. E. J. and Offringa, R.** (2014). PIN-driven polar auxin transport in
725 plant developmental plasticity: a key target for environmental and
726 endogenous signals. *New Phytologist* **203**, 362–377.
- 727 **Heisler, M. G., Ohno, C., Das, P., Sieber, P., Reddy, G. V., Long, J. A. and**
728 **Meyerowitz, E. M.** (2005). Patterns of auxin transport and gene expression
729 during primordium development revealed by live imaging of the Arabidopsis
730 inflorescence meristem. *Curr Biol* **15**, 1899–1911.
- 731 **Jia, W., Li, B., Li, S., Liang, Y., Wu, X., Ma, M., Wang, J., Gao, J., Cai, Y.,**
732 **Zhang, Y., et al.** (2016). Mitogen-Activated Protein Kinase Cascade MKK7-
733 MPK6 Plays Important Roles in Plant Development and Regulates Shoot
734 Branching by Phosphorylating PIN1 in Arabidopsis. *PLoS Biol* **14**,
735 e1002550.
- 736 **Jönsson, H., Heisler, M. G., Shapiro, B. E., Meyerowitz, E. M. and**
737 **Mjolsness, E.** (2006). An auxin-driven polarized transport model for
738 phyllotaxis. *Proc Natl Acad Sci USA* **103**, 1633–1638.
- 739 **Kierzkowski, D., Lenhard, M., Smith, R. S. and Kuhlemeier, C.** (2013).
740 Interaction between meristem tissue layers controls phyllotaxis. *Dev Cell* **26**,
741 616–628.
- 742 **Kleine-Vehn, J., Dhonukshe, P., Sauer, M., Brewer, P. B., Wisniewska, J.,**
743 **Paciorek, T., Benková, E. and Friml, J.** (2008). ARF GEF-dependent

- 744 transcytosis and polar delivery of PIN auxin carriers in Arabidopsis. *Curr Biol*
745 **18**, 526–531.
- 746 **Knöller, A. S., Blakeslee, J. J., Richards, E. L., Peer, W. A. and Murphy, A.**
747 **S.** (2010). Brachytic2/ZmABCB1 functions in IAA export from intercalary
748 meristems. *J Exp Bot* **61**, 3689–3696.
- 749 **Lenhard, M.** (2003). Stem cell homeostasis in the Arabidopsis shoot meristem
750 is regulated by intercellular movement of CLAVATA3 and its sequestration
751 by CLAVATA1. *Development* **130**, 3163–3173.
- 752 **Leyser, H. M. O.** (2005). Auxin Distribution and Plant Pattern Formation: How
753 Many Angels Can Dance on the Point of PIN? *Cell* **121**, 819–822.
- 754 **Leyser, H. M. O.** (2006). Dynamic integration of auxin transport and signalling.
755 *CURBIO* **16**, R424–33.
- 756 **Leyser, H. M. O.** (2010). The power of auxin in plants. *Plant Physiol* **154**, 501–
757 505.
- 758 **Luschig, C. and Vert, G.** (2014). The dynamics of plant plasma membrane
759 proteins: PINs and beyond. *Development* **141**, 2924–2938.
- 760 **Martinez, C. C., Koenig, D., Chitwood, D. H. and Sinha, N. R.** (2016). A sister
761 of PIN1 gene in tomato (*Solanum lycopersicum*) defines leaf and flower
762 organ initiation patterns by maintaining epidermal auxin flux. *Dev Biol* **419**,
763 85–98.
- 764 **Miao, J., Guo, D., Zhang, J., Huang, Q., Qin, G., Zhang, X., Wan, J., Gu, H.**
765 **and Qu, L.-J.** (2013). Targeted mutagenesis in rice using CRISPR-Cas
766 system. *Cell Res* **23**, 1233–1236.
- 767 **Mitchison, G. J.** (1980). A Model for Vein Formation in Higher Plants. *Proc.*
768 *Biol. Sci.* **207**, 79–109.
- 769 **Mitchison, G. J., Hanke, D. E. and Sheldrake, A. R.** (1981). The Polar
770 Transport of Auxin and Vein Patterns in Plants [and Discussion].
771 *Philosophical Transactions of the Royal Society B: Biological Sciences* **295**,
772 461–471.
- 773 **Moore, I., Gälweiler, L., Grosskopf, D. and Palme, K.** (1998). A transcription
774 activation system for regulated gene expression in transgenic plants. *Proc.*
775 *Natl. Acad. Sci. U.S.A.* **95**, 376–381.
- 776 **O'Connor, D. L., Runions, A., Runions, A., Sluis, A., Sluis, A., Bragg, J.,**
777 **Bragg, J., Vogel, J. P., Vogel, J. P., Prusinkiewicz, P., et al.** (2014). A
778 division in PIN-mediated auxin patterning during organ initiation in grasses.
779 **10**, e1003447.

- 780 **Okada, K.** (1991). Requirement of the Auxin Polar Transport System in Early
781 Stages of Arabidopsis Floral Bud Formation. *THE PLANT CELL ONLINE* **3**,
782 677–684.
- 783 **Paponov, I. A., Teale, W. D. and Trebar, M.** (2005). The PIN auxin efflux
784 facilitators: evolutionary and functional perspectives. *Trends Plant Sci* **10**,
785 170–177.
- 786 **Prusinkiewicz, P., Crawford, S., Smith, R. S., Ljung, K., Bennett, T. A.,**
787 **Ongaro, V. and Leyser, H. M. O.** (2009). Control of bud activation by an
788 auxin transport switch. *Proc Natl Acad Sci USA* **106**, 17431–17436.
- 789 **Raven, J. A.** (1975). Transport of indoleacetic acid in plant cells in relation to
790 pH and electrical potential gradients, and its significance for polar IAA
791 transport. *New Phytol* **74**, 163–172.
- 792 **Reinhardt, D., Mandel, T. and Kuhlemeier, C.** (2000). Auxin Regulates the
793 Initiation and Radial Position of Plant Lateral Organs. *The Plant Cell* **12**, 507.
- 794 **Reinhardt, D., Pesce, E.-R., Stieger, P., Mandel, T., Baltensperger, K.,**
795 **Bennett, M. J., Traas, J., Friml, J. and Kuhlemeier, C.** (2003). Regulation
796 of phyllotaxis by polar auxin transport. *Nature* **426**, 255–260.
- 797 **Rubery, P. H. and Sheldrake, A. R.** (1974). Carrier-mediated auxin transport.
798 *Planta* **118**, 101–121.
- 799 **Sawchuk, M. G., Edgar, A. and Scarpella, E.** (2013). Patterning of Leaf Vein
800 Networks by Convergent Auxin Transport Pathways. *PLoS Genet* **9**,
801 e1003294.
- 802 **Scarpella, E., Marcos, D., Friml, J. and Berleth, T.** (2006). Control of leaf
803 vascular patterning by polar auxin transport. *Genes Dev* **20**, 1015–1027.
- 804 **Sessions, A., Weigel, D. and Yanofsky, M. F.** (2002). The Arabidopsis
805 thaliana MERISTEM LAYER 1 promoter specifies epidermal expression in
806 meristems and young primordia. *Plant J* **20**, 259–263.
- 807 **Shinohara, N., Taylor, C. and Leyser, H. M. O.** (2013). Strigolactone Can
808 Promote or Inhibit Shoot Branching by Triggering Rapid Depletion of the
809 Auxin Efflux Protein PIN1 from the Plasma Membrane. *PLoS Biol* **11**,
810 e1001474.
- 811 **Smith, R. S.** (2006). A plausible model of phyllotaxis. *Proc Natl Acad Sci USA*
812 **103**, 1301–1306.
- 813 **Stoma, S., Lucas, M., Chopard, J., Schaedel, M. and Godin, C.** (2008). Flux-
814 Based Transport Enhancement as a Plausible Unifying Mechanism for
815 Auxin Transport in Meristem Development. *PLoS Comput Biol* **4**, e1000207.

- 816 **Verna, C., Sawchuk, M. G., Linh, N. M. and Scarpella, E.** (2015). Control of
817 vein network topology by auxin transport. *BMC Biol* **13**, 94.
- 818 **Vieten, A., Vanneste, S., Wisniewska, J., Benkova, E., Benjamins, R.,**
819 **Beeckman, T., Luschnig, C. and Friml, J.** (2005). Functional redundancy
820 of PIN proteins is accompanied by auxin-dependent cross-regulation of PIN
821 expression. *Development* **132**, 4521–4531.
- 822 **Willige, B. C., Ahlers, S., Zourelidou, M., Barbosa, I. C. R., Demarsy, E.,**
823 **Trevisan, M., Davis, P. A., Roelfsema, M. R. G., Hangarter, R.,**
824 **Fankhauser, C., et al.** (2013). D6PK AGCVIII kinases are required for auxin
825 transport and phototropic hypocotyl bending in *Arabidopsis*. *The Plant Cell*
826 **25**, 1674–1688.
- 827 **Wisniewska, J., Xu, J., Seifertová, D., Brewer, P. B., Ruzicka, K., Blilou, I.,**
828 **Rouquié, D., Benková, E., Scheres, B. and Friml, J.** (2006). Polar PIN
829 localization directs auxin flow in plants. *Science* **312**, 883–883.
- 830 **Xu, J., Hofhuis, H., Heidstra, R., Sauer, M., Friml, J. and Scheres, B.** (2006).
831 A molecular framework for plant regeneration. *Science* **311**, 385–388.
- 832 **Zhou, C., Han, L., Hou, C., Metelli, A., Qi, L., Tadege, M., Mysore, K. S. and**
833 **Wang, Z.-Y.** (2011). Developmental analysis of a *Medicago truncatula*
834 smooth leaf margin1 mutant reveals context-dependent effects on
835 compound leaf development. *The Plant Cell* **23**, 2106–2124.
- 836 **Zourelidou, M., Absmanner, B., Weller, B., Barbosa, I. C. R., Willige, B. C.,**
837 **Fastner, A., Streit, V., Port, S. A., Colcombet, J., la Fuente van Bentem,**
838 **de, S., et al.** (2014). Auxin efflux by PIN-FORMED proteins is activated by
839 two different protein kinases, D6 PROTEIN KINASE and PINOID. *eLife* **3**.
- 840
- 841

842 **Figures and Legends**

843

844 **Figure 1. SoPIN1 and PIN1b have different functions in Brachypodium. (A)**
845 SoPIN1 (Bradi4g26300) and PIN1b (Bradi3g59520) CRISPR-derived *sopin1-1* and
846 *pin1b-1* mutant alleles. Exons are indicated by grey boxes. Arrowheads indicate
847 CRISPR target sites and are labeled with the type of DNA lesion (C insertion or A
848 deletion). Both alleles have premature stop codons at the positions indicated by lines.
849 **(B-D)** Inflorescence phenotypes of CRISPR-derived *sopin1-1* and *pin1b-1* mutants.
850 **(B)** Wildtype (WT) (inbred line Bd21-3) Brachypodium inflorescences usually have
851 several spikelets (s) on each inflorescence. Inset shows spikelet meristem (arrow),
852 with several floral meristems being initiated. **(C)** *sopin1-1* plants have severe organ
853 initiation defects in the inflorescence, and spikelets often abort (asterisk), or fail to
854 initiate despite a clear distinction between the white node (n) and green internode (i)
855 tissue. Inset shows two barren spikelet meristems (arrows) with organ initiation
856 defects. **(D)** *pin1b-1* plants have normal organ initiation, but internode tissue often
857 bends. A phenotypically normal spikelet (s) is indicated. **(E)** Medial confocal Z-section
858 of pZmUbi::DII-Venus (DII) expression in a WT spikelet co-expressing SoPIN1 tagged
859 with Cerulean (a CFP variant) under the native SoPIN1 promoter. Organ primordia are
860 numbered I3, I2, I1 from youngest to oldest prior to morphogenesis, and P1, P2, P3,
861 etc. youngest to oldest after morphogenesis. DII is normally degraded at SoPIN1
862 convergence points in I2 and I1 primordia (asterisks). Inset shows color look-up-table
863 for all PIN images. **(F)** Medial confocal Z-section of pZmUbi::DII-Venus expression in
864 a *sopin1-1* spikelet meristem. DII degradation does not occur in *sopin1-1* meristems,
865 and organs fail to initiate (arrow). Inset shows color look-up-table for DII. **(G-H)** Basal
866 internodes are elongated in *pin1b-1* mutants compared to WT. Lines in **(G)** connect
867 equivalent nodes in WT (left) and *pin1b-1* (right) primary stems. Axillary shoots and
868 leaves have been removed from the main axis. **(H)** Mean internode lengths along WT
869 (left) and *pin1b-1* (right) primary stems. Nodes are numbered from 1 starting from
870 below the inflorescence. (n=11-12 each internode, error bars +/- standard error of the
871 mean). **(I)** Maximum projection of PIN1b tagged with Citrine under its native promoter
872 in a longitudinal hand-section through several immature vegetative nodes. Arrows
873 indicate the shoot apical meristem (SAM), node (n), and internode (i) tissues. Scale
874 bars: 1cm in **(B-D)** and **(G)**. 25µm in **(E)**, **(F)** and **(I)**.

875

876 **Figure 1 – supplement 1. Mature whole-plant phenotypes of Brachypodium**
877 **CRISPR-derived *sopin1-1* and *pin1b-1* mutants.** Left WT (Inbred Bd21-3), middle
878 *sopin1-1*, and right *pin1b-1*. Scale bar: 1cm.

879

880 **Figure 1 – supplement 2. DII-Venus is degraded in the presence of auxin in**
881 **Brachypodium spikelet meristems. (A)** 1 µM NAA-treated, and **(B)** mock-treated
882 spikelet meristems expressing pZmUbi::DII-Venus imaged every 30 min after
883 treatment. Images from left to right, pre-treatment expression, 30 min, 60 min and 90
884 min time-points. Scale bars: 25µm.

885

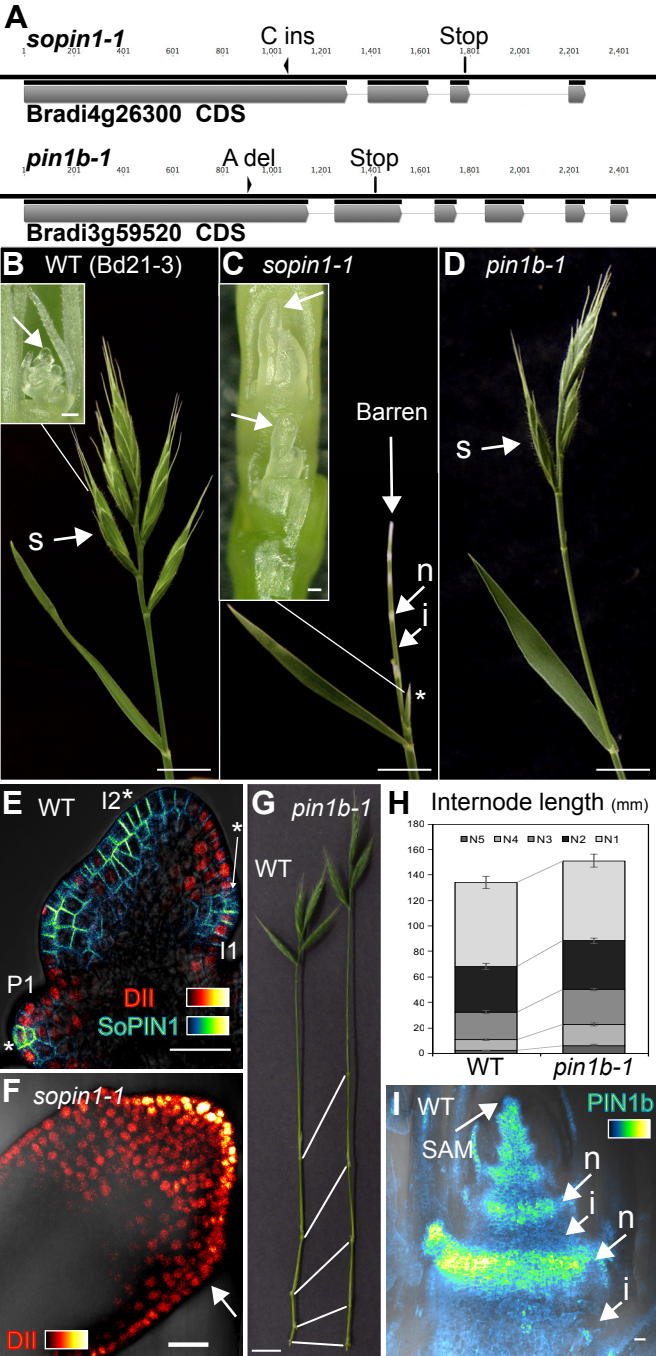


Figure 1

WT (Bd21-3)

sopin1-1

pin1b-1

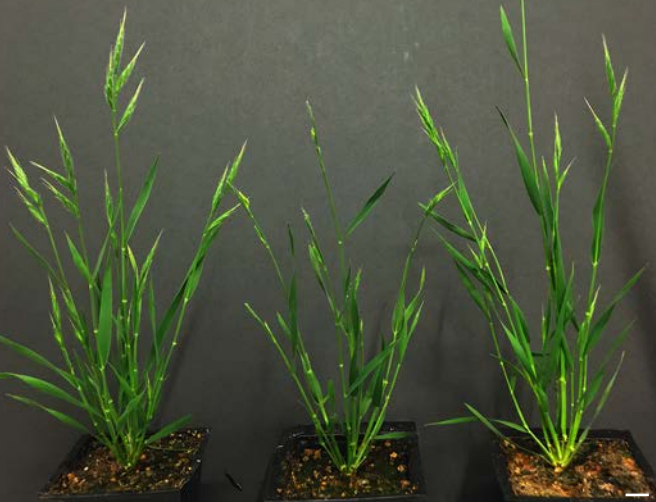


Figure 1 - supplement 1

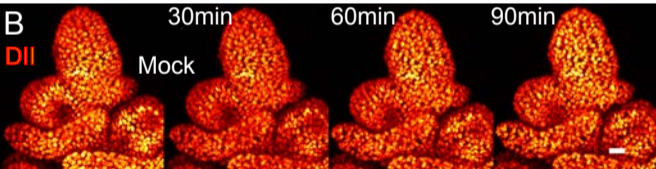
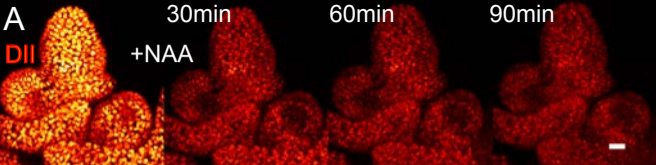


Figure 1 - supplement 2

886 **Figure 2. SoPIN1 and PIN1b show different behaviors when expressed in**
887 **wildtype Arabidopsis.** Arabidopsis *AtPIN1* promoter (*proAtPIN1*) -driven expression
888 of Citrine-tagged (a YFP derivative) SoPIN1 and PIN1b in wildtype Columbia (Col-0)
889 Arabidopsis. **(A,C,E,G,I,J,K)** SoPIN1, **(B,D,F,H,L,M)** PIN1b. **(A-B)** Maximum
890 projections of meristem apices. Arrow in **(A)** indicates SoPIN1 convergence point (cp)
891 in an I2 primordium. Arrow in **(B)** indicates internalized PIN1b in punctate membrane
892 bodies. **(C-D)** Tiled confocal maximum projections of longitudinal hand-sections
893 through apices. Arrows indicate SoPIN1 epidermal expression in sepal primordia and
894 flower pedicels in **(C)** and the lack of PIN1b epidermal expression in the same tissues
895 in **(D)**. **(E-F)** Tiled confocal maximum projections of longitudinal sections through basal
896 inflorescence stem internodes 1cm above the rosette. **(G-H)** Tiled confocal maximum
897 projections of cross-sections through basal internodes 1cm above the rosette. Signal
898 at the edge of each section (arrows) is cuticle auto-fluorescence. The cambium (c),
899 xylem parenchyma (xp), and pith (p) tissues are indicated in **(E-H)**. **(I)** Maximum
900 projection detail of SoPIN1 convergence point (Asterisk) in I2 primordia in meristem
901 shown in **(A)**. **(J)** Confocal z-section of SoPIN1 accumulation in a ring-shaped domain
902 just below the apex of the meristem shown in **(A)**. **(K)** Maximum projection detail of
903 root-ward polarized SoPIN1 (arrows) in a longitudinal section of the basal internode
904 pith tissue. **(L)** Confocal z-section of PIN1b accumulation in distinct vascular-
905 associated domains just below the apex of the meristem shown in **(B)**. **(M)** Maximum
906 projection detail of root-ward polarized PIN1b (arrows) in a longitudinal section of the
907 basal internode xylem parenchyma tissue. Red signal in all panels is chlorophyll auto-
908 fluorescence. Scale bars: 25µm in **(A-B)**, 100µm in **(C-H)**, and 25µm in **(I-M)**.
909

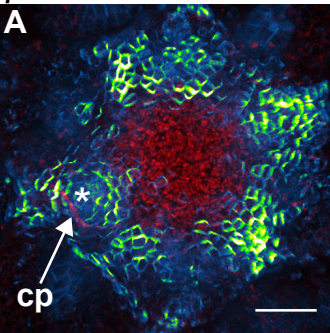
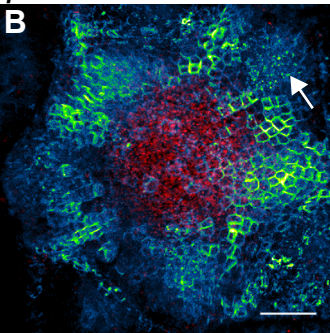
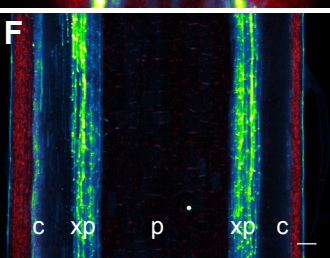
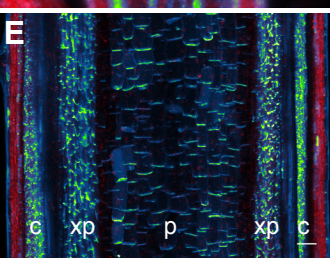
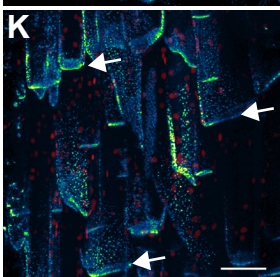
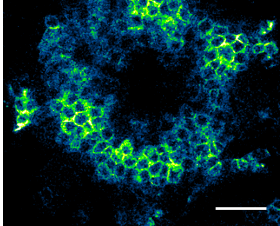
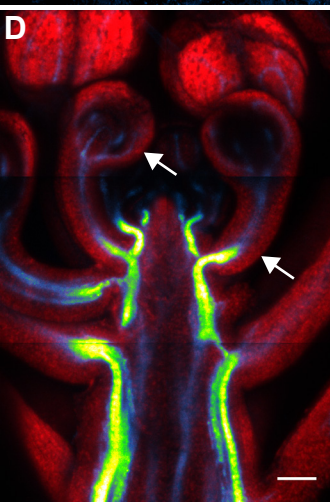
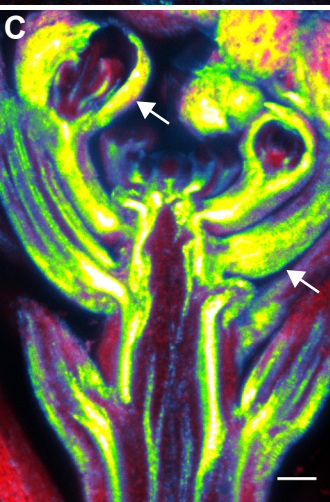
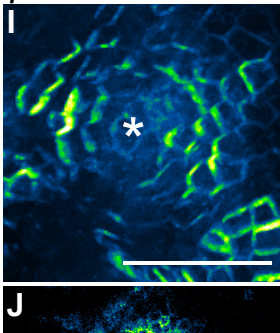
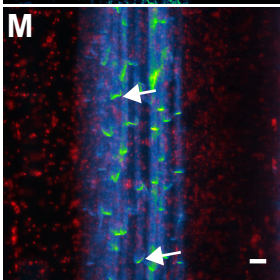
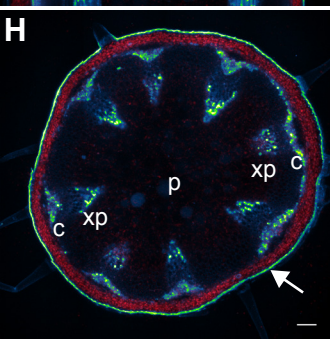
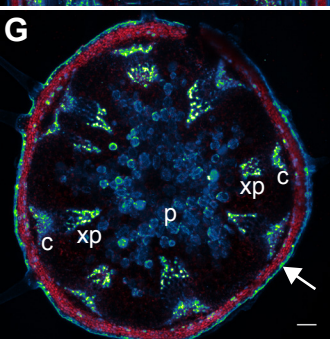
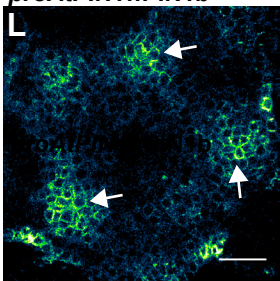
proAtPIN1::SoPIN1*proAtPIN1::PIN1b**proAtPIN1::SoPIN1**proAtPIN1::PIN1b*

Figure 2

910 **Figure 3. SoPIN1 but not PIN1b can partially complement the Arabidopsis *pin1-***
911 ***613* mutant organ initiation and bulk transport defects. (A)** From left to right,
912 inflorescence phenotypes of WT (Col-0), *proAtPIN1::SoPIN1* in *pin1-613*,
913 *proAtPIN1::PIN1b* in *pin1-613*, and *pin1-613* alone. Note that PIN1b-expressing *pin1-*
914 *613* plants are indistinguishable from *pin1-613* alone. **(B)** Flower (left), and
915 inflorescence apex (right) of WT (Col-0). **(C)** Flower (left), and inflorescence apex
916 (right) of *proAtPIN1::SoPIN1* complemented *pin1-613* mutants. Note the increase in
917 petal number in the flower, see Figure 3 - supplement 2 for organ counts. **(D)** Box-plot
918 of bulk auxin transport (counts per minute, CPM) through basal internodes 1cm above
919 the rosette of 40-day-old Arabidopsis inflorescence stems. (n=16 each genotype).
920 Samples with different letters are significantly different from each other (ANOVA,
921 Tukey HSD, $p < 0.05$). Scale bars: 1cm in **(A)**, 1mm in **(B-C)**.

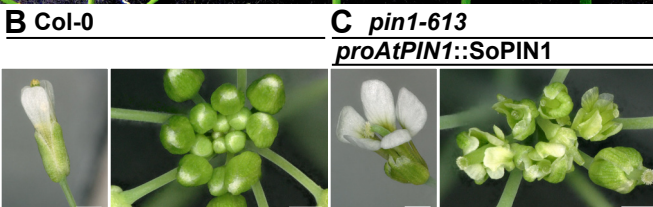
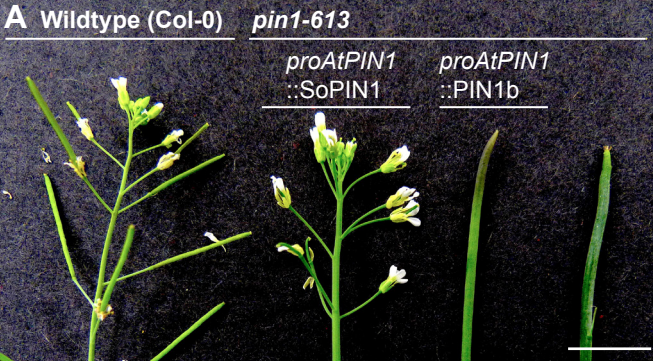
922

923 **Figure 3 - supplement 1. Whole-plant phenotypes of *proAtPIN1*-driven**
924 **complementation of *pin1-613*.** From left to right, Col-0, *proAtPIN1::SoPIN1*
925 complemented *pin1-613*, *proAtPIN1::PIN1b* expressing *pin1-613*, *pin1-613*.

926

927 **Figure 3 - supplement 2. Floral organ number in *proAtPIN1::SoPIN1***
928 **complemented flowers.** Mean and standard-error of sepal, petal, stamen and carpel
929 organ numbers in heterozygous *pin1-613* or wildtype (white bars), and
930 *proAtPIN1::SoPIN1*-complemented *pin1-613* flowers (grey bars) (n=30).

931



D Stem auxin transport

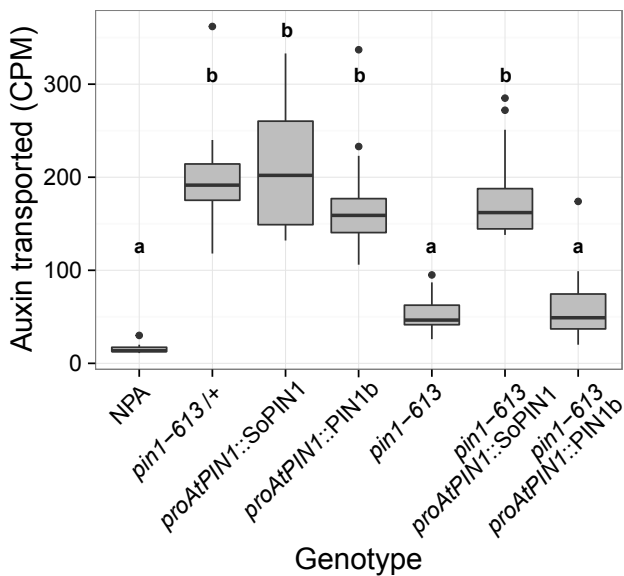


Figure 3

Col-0

pin1-613

proAtPIN1
::*SoPIN1*

proAtPIN1
::*PIN1b*

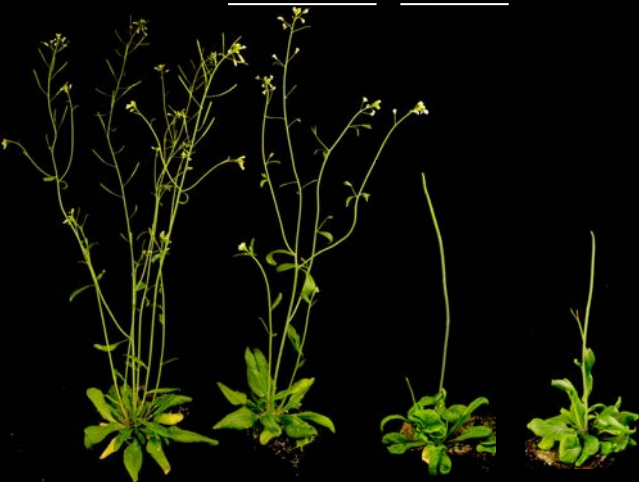


Figure 3 - supplement 1

Floral organ number - *proAtPIN1::SoPIN1*

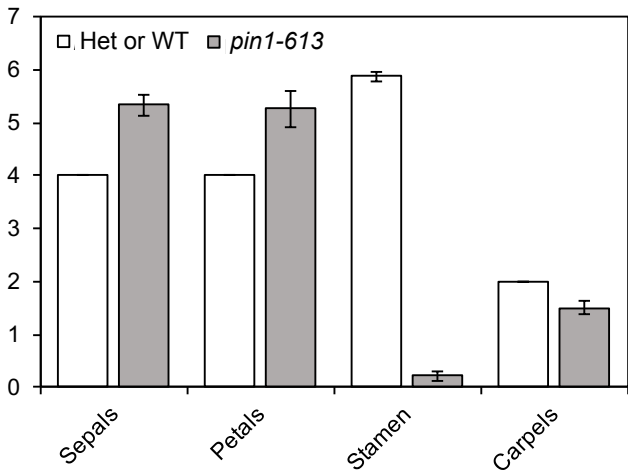


Figure 3 - supplement 2

932 **Figure 4. SoPIN1 but not PIN1b can mediate organ initiation and bulk transport**
933 **in null *pin1-613* mutants.** Arabidopsis *PIN1* promoter (*proAtPIN1*) -driven expression
934 of Citrine-tagged (YFP derivative) SoPIN1 and PIN1b in null *pin1-613* mutant tissue.
935 **(A,C,E,G,I)** SoPIN1, **(B,D,F,H,J,K,L,M)** PIN1b. **(A-B)** Maximum projections of
936 meristem apices. Arrow in **(B)** indicates PIN1b ring shaped epidermal domain. **(C-D)**
937 Tiled confocal maximum projections of longitudinal hand-sections through apices.
938 Arrow in **(D)** indicates increased PIN1b in the epidermis in the *pin1-613* background.
939 **(E-F)** Tiled maximum projections of longitudinal sections through basal inflorescence
940 stem internodes 1cm above the rosette. **(G-H)** Tiled maximum projections of cross-
941 sections through basal internodes 1cm above the rosette. Signal at the edge of each
942 section (arrows) is cuticle auto-florescence. The cambium (c), xylem parenchyma (xp),
943 and pith (p) tissues are indicated in **(E-H)**. **(I)** Confocal z-section of SoPIN1
944 accumulation in a ring-shaped domain just below the apex of a complemented *pin1-*
945 *613* meristem. **(J)** Longitudinal hand-section of PIN1b just below a *pin1-613* meristem
946 apex. Arrow shows root-ward polarized PIN1b. **(K)** Detail of polarized PIN1b in the
947 meristem epidermis of a *pin1-613* meristem apex. **(L)** Cross-section of PIN1b in
948 distinct bundles 2mm below a *pin1-613* meristem apex. **(M)** Root-ward polarization of
949 PIN1b (arrow) 3-4 mm below the apex of a *pin1-613* meristem. Red signal in all panels
950 is chlorophyll auto-florescence. Scale bars: 25µm in **(A-B)**, 100µm in **(C-H)**, and 25µm
951 in **(I-M)**.

952

953 **Figure 4 – supplement 1. *proAtPIN1*-driven SoPIN1 expression in *pin1-613***
954 **segregating family. (A)** *proAtPIN1::SoPIN1* expression in 6 different wt or het *pin1-*
955 *613* meristem samples. **(B)** *proAtPIN1::SoPIN1* expression in 6 different
956 complemented *pin1-613* meristems. All samples were imaged with identical settings
957 to show the increase in SoPIN1 in the *pin1-613* mutant background. Red signal is
958 chlorophyll auto-florescence. Scale bars: 25µm.

959

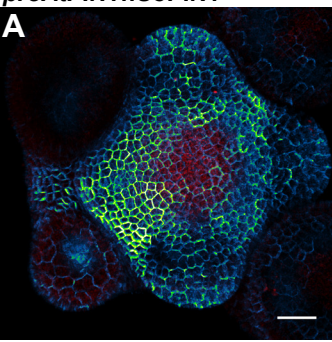
960 **Figure 4 – supplement 2. *proAtPIN1*-driven PIN1b expression in *pin1-613***
961 **apexes.** Two representative meristems each from four different transgenic events. All
962 samples were imaged with identical settings. Scale bars: 25µm.

963

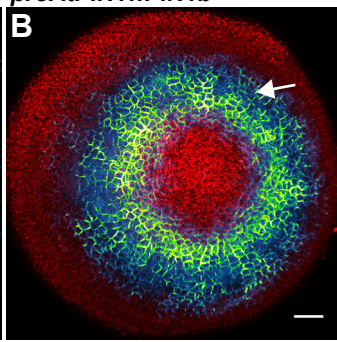
964 **Figure 4 – supplement 3. *proAtPIN1*-driven PIN1b dynamics during organ**
965 **formation induced by addition of lanolin containing 1mM IAA on *pin1-613***
966 **apexes.** From left to right, pre-treatment, 24, 48, 72, and 96 hours after treatment.
967 Four representative samples are shown top to bottom. Arrows indicate the lanolin
968 paste at the 24-hour time-point. All samples were imaged with identical settings. Scale
969 bars 25µm.

970

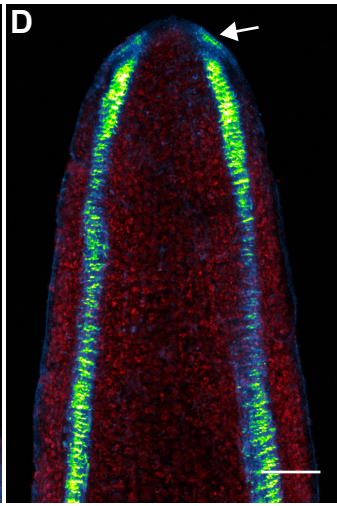
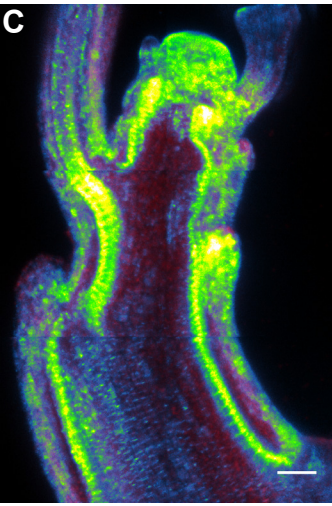
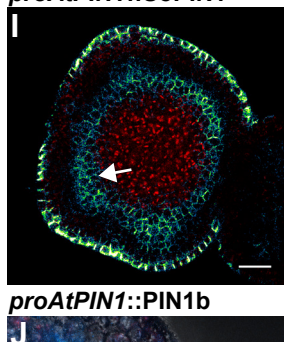
proAtPIN1::SoPIN1



proAtPIN1::PIN1b



proAtPIN1::SoPIN1



proAtPIN1::PIN1b

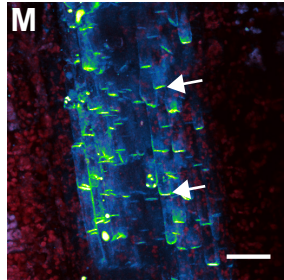
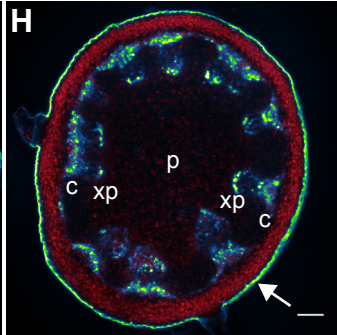
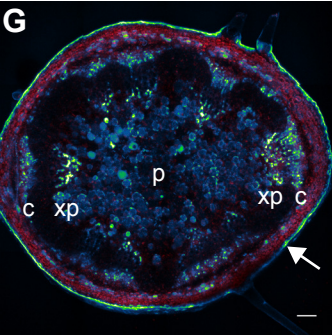
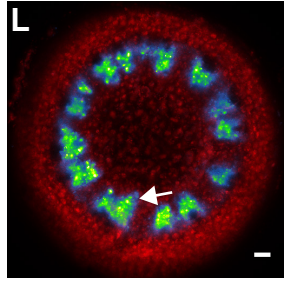
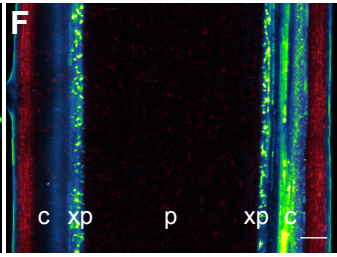
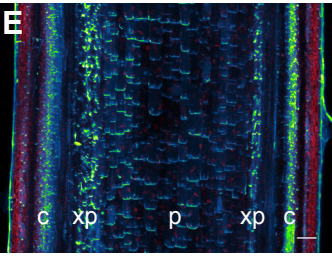
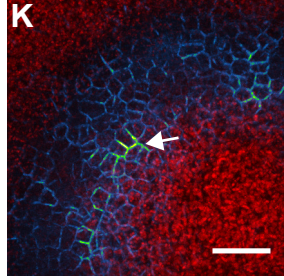
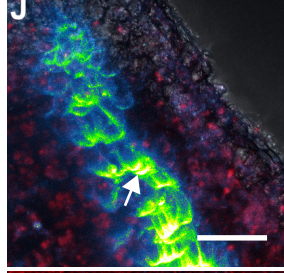
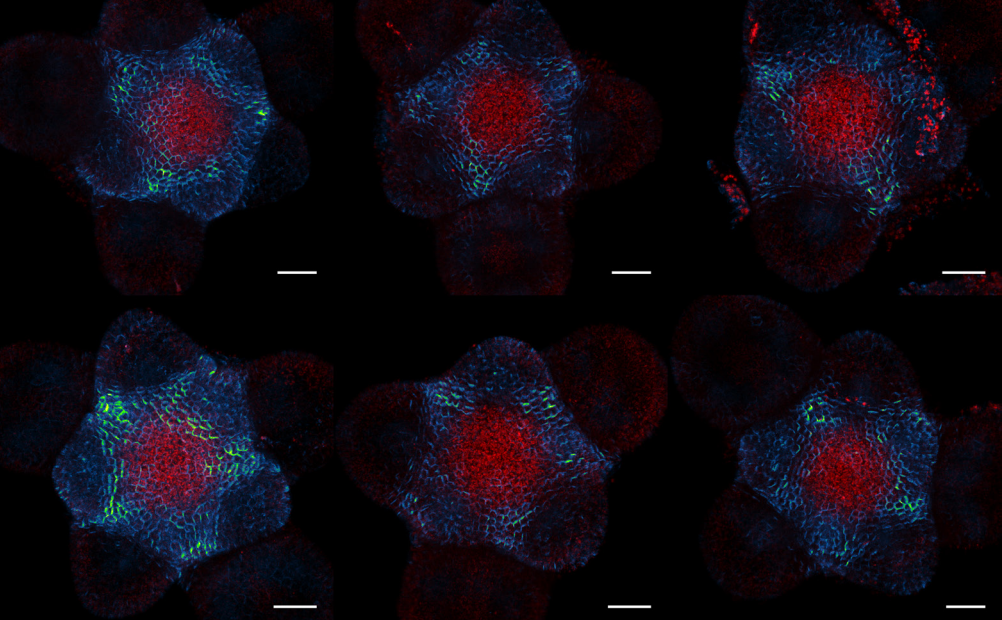


Figure 4

A *proAtPIN1::SoPIN1* WT or heterozygous



B *proAtPIN1::SoPIN1* complemented *pin1-613*

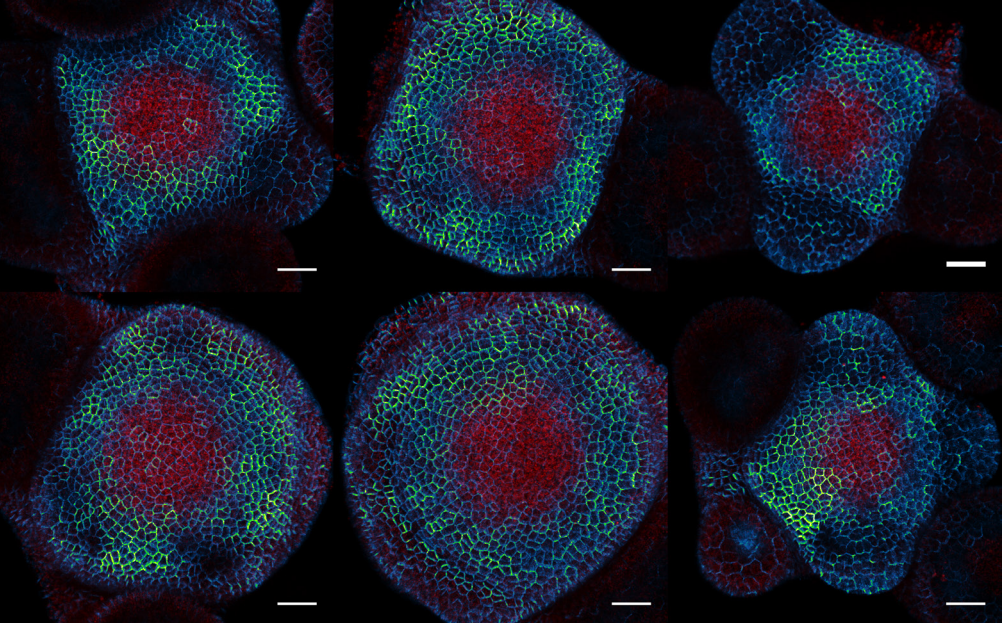
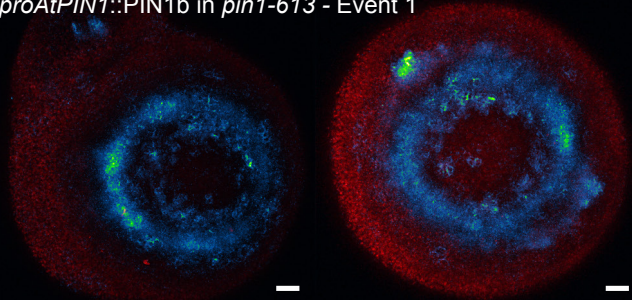
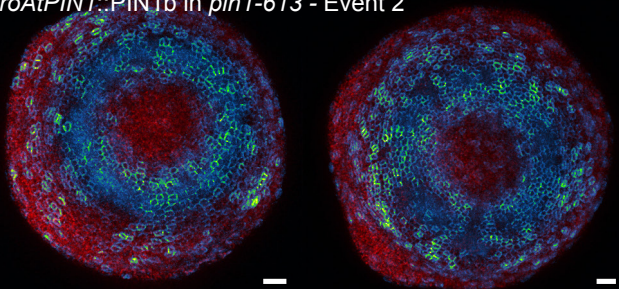


Figure 4 - supplement 1

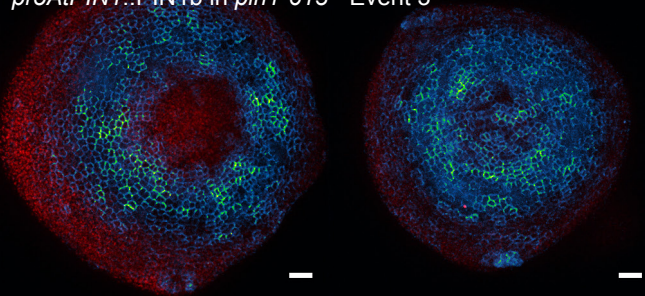
proAtPIN1::PIN1b in *pin1-613* - Event 1



proAtPIN1::PIN1b in *pin1-613* - Event 2



proAtPIN1::PIN1b in *pin1-613* - Event 3



proAtPIN1::PIN1b in *pin1-613* - Event 4

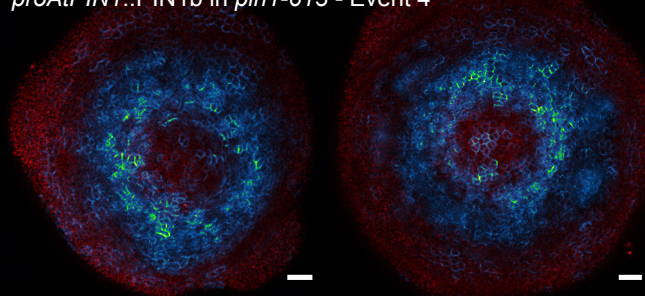


Figure 4 - supplement 2

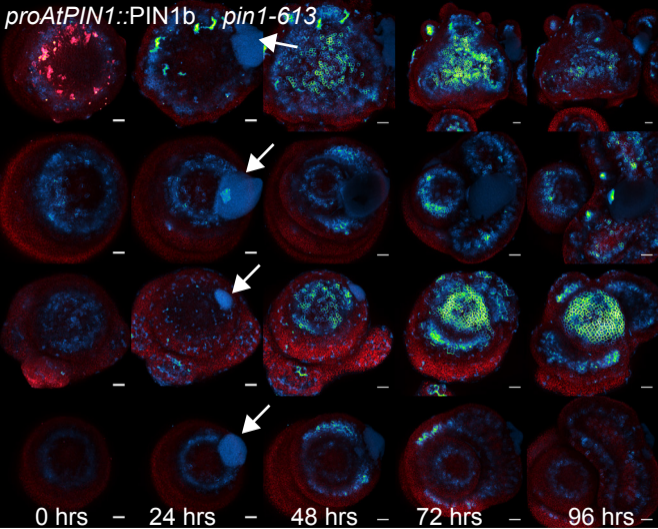


Figure 4 - supplement 3

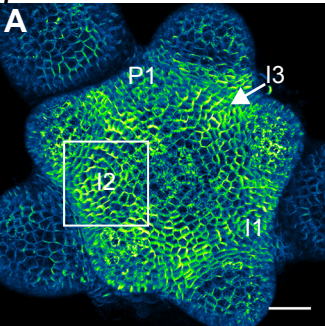
971 **Figure 5. SoPIN1 and PIN1b show different behaviors under *proAtML1*-driven**
972 **expression.** Maximum projections of *proAtML1::LhG4* driving pOP::SoPIN1 or
973 pOP::PIN1b (*proAtML1>>SoPIN1* and *proAtML1>>PIN1b*) in wildtype Landsberg
974 *erecta* (*Ler*) (**A-D**), and *pin1-4* (**E-L**) inflorescence meristems and basal internodes.
975 **(A)** SoPIN1 and **(B)** PIN1b maximum projections of wildtype *Ler* inflorescence
976 meristems. I3, I2, I1, and P1 primordia are indicated. White boxes around each I2
977 primordium indicate the regions detailed in **(C-D)**. Asterisk in **(C)** indicates
978 convergence point. Arrow in **(D)** indicates punctate PIN1b. **(E)** SoPIN1 and **(F)** PIN1b
979 maximum projections of complemented *pin1-4* meristems. I3, I2, I1, and P1 primordia
980 are indicated. White boxes around each I2 primordia indicate the regions detailed in
981 **(G-H)**. Asterisks mark convergence points in **(G)** and **(H)**. Red signal in **(C,D,G,H)** is
982 cell wall propidium iodide staining. **(I-J)** Tiled maximum projections of cross hand-
983 sections of the basal internode of SoPIN1 **(I)** and PIN1b **(J)** -complemented *pin1-4*
984 plants showing PIN signal in the outer cortex layers (arrows). Red signal in **(I-J)** is
985 chlorophyll auto-fluorescence. **(K-L)** Epidermal maximum projections showing root-
986 ward polarized PIN localization (arrows) in the basal internode of SoPIN1 **(K)**, and
987 PIN1b **(L)** -complemented *pin1-4* plants. Scale bars: 25µm in **(A-H)**. 100µm in **(I-L)**.
988

989 **Figure 5 – supplement 1. *proAtML1>>SoPIN1* representative meristem maximum**
990 **projections.** **(A)** *proAtML1>>SoPIN1* expression in three different wildtype *Ler*
991 meristems. **(B)** *proAtML1>>SoPIN1* expression in three different complemented *pin1-*
992 *4* meristems. Capture settings are identical in all samples. Scale bars: 25µm.
993

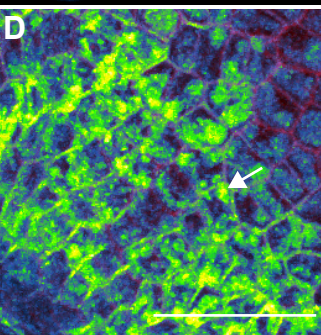
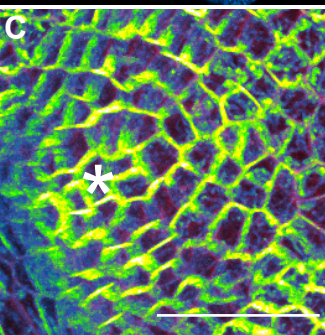
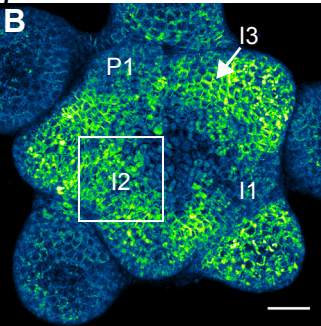
994 **Figure 5 – supplement 2. *proAtML1>>PIN1b* representative meristem maximum**
995 **projections.** **(A)** *proAtML1>>PIN1b* expression in three different wildtype *Ler*
996 meristems. **(B)** *proAtML1>>PIN1b* expression in three different complemented *pin1-*
997 *4* meristems. Capture settings are identical in all samples. Scale bars: 25µm.
998

Wildtype (Ler)

proAtML1>>SoPIN1

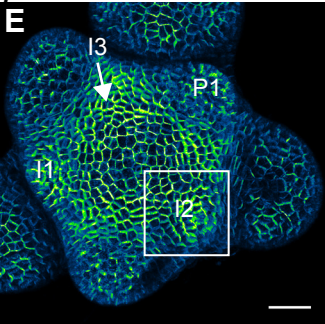


proAtML1>>PIN1b



pin1-4

proAtML1>>SoPIN1



proAtML1>>PIN1b

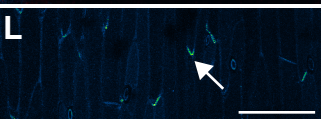
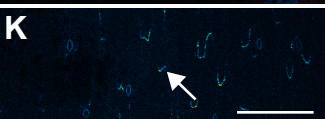
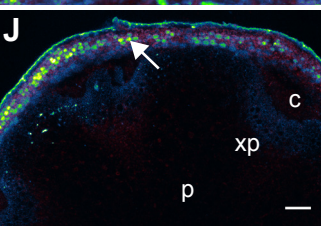
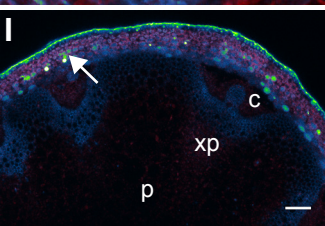
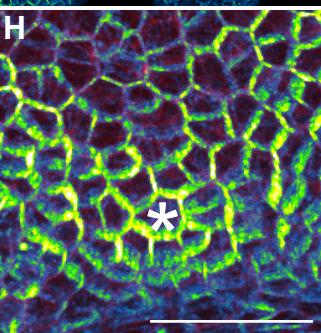
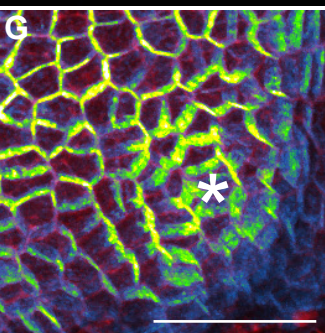
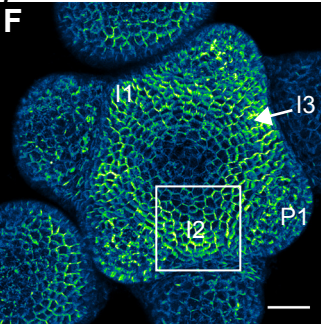
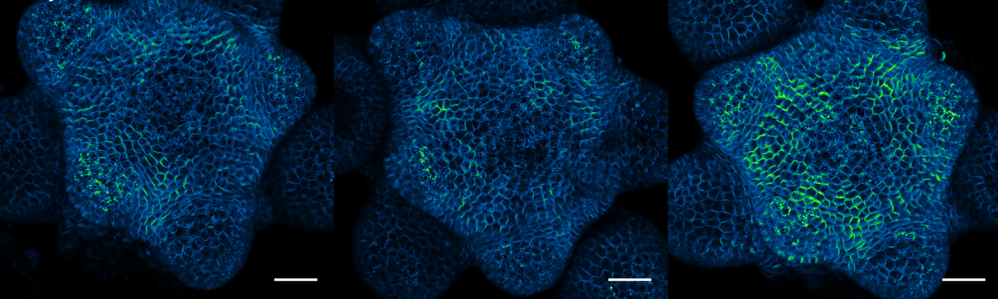


Figure 5

A *proAtML1>>SoPIN1* WT



B *proAtML1>>SoPIN1 pin1-4*

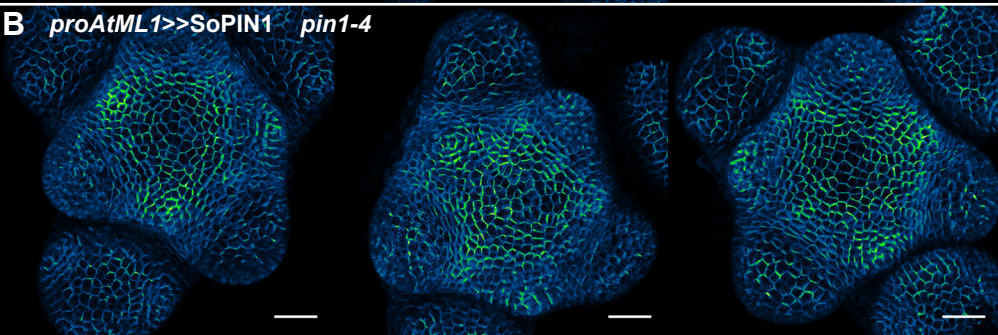
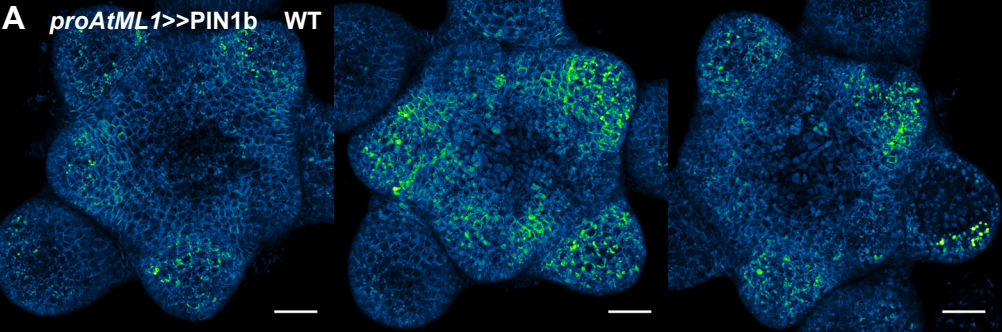


Figure 5 - supplement 1 - *proAtML1>>SoPIN1*

A *proAtML1>>PIN1b* WT



B *proAtML1>>PIN1b pin1-4*

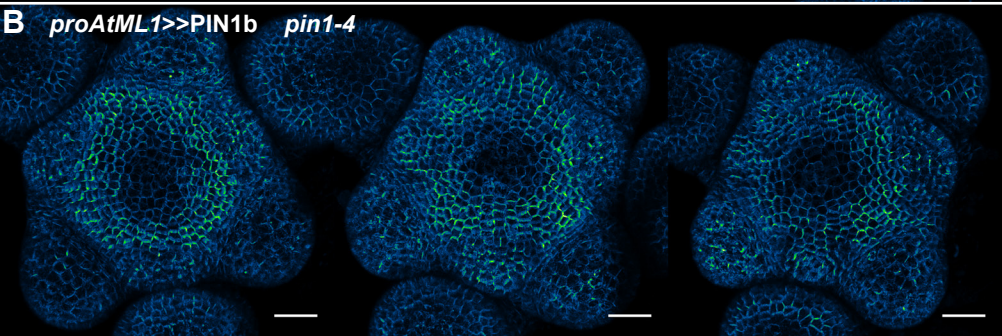
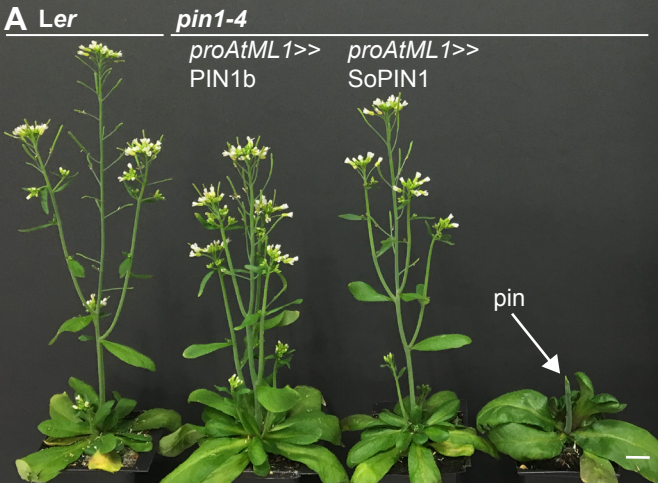


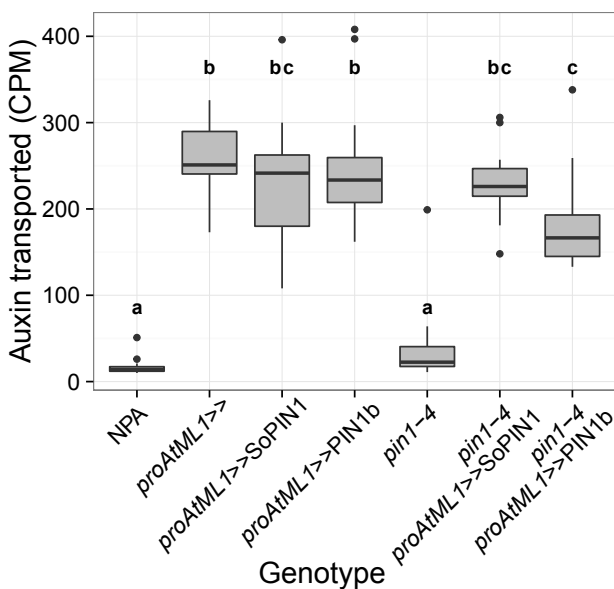
Figure 5 - supplement 2 - *proAtML1>>PIN1b*

999 **Figure 6. Both SoPIN1 and PIN1b can complement *Arabidopsis pin1-4* under**
1000 ***proAtML1*-driven expression. (A)** From left to right, wildtype *Ler*, *proAtML1>>*PIN1b
1001 complemented *pin1-4*, *proAtML1>>*SoPIN1 complemented *pin1-4*, and *pin1-4* alone.
1002 Arrow indicates barren pin inflorescence in *pin1-4*. **(B)** Box-plot of bulk auxin transport
1003 (counts per minute, CPM) through basal internodes 1cm above the rosette of 40-day-
1004 old *Arabidopsis* inflorescence stems (n=16 each genotype). Samples with different
1005 letters are significantly different from each other (ANOVA, Tukey HSD, p < 0.05). **(C)**
1006 Box-plot of stem cross-sectional area (square mm) of the basal internode 1cm above
1007 the rosette (n=12 each genotype). Representative Toluidine Blue O stained hand
1008 cross-sections are shown above each box. Samples with different letters are
1009 significantly different from each other. (ANOVA, Tukey HSD, p < 0.05). *Scale bars:*
1010 1cm in **(A)**. 500µm in **(C)**.

1011
1012 **Figure 6 – supplement 1. *proAtML1>>* complemented *pin1-4* inflorescence**
1013 **phenotypes. (A)** Wildtype *Ler*, **(B)** *proAtML1>>*SoPIN1 complemented *pin1-4*, and
1014 **(C)** *proAtML1>>*PIN1b complemented *pin1-4* inflorescence apices. *Scale bars:* 1mm.
1015



B Stem auxin transport



C Stem cross-sectional area

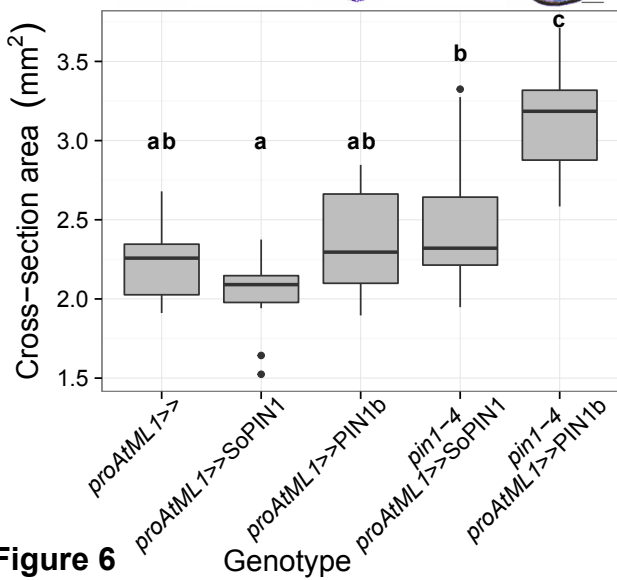
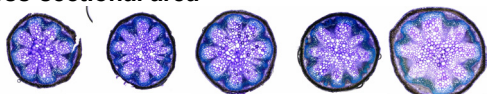


Figure 6

A *Ler*



B *pin1-4*

proAtML1>>SoPIN1



C

proAtML1>>PIN1b

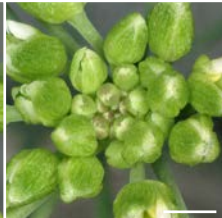


Figure 6 - supplement 1

1016 **Figure 7. Heterologous expression summary: Functional distinction between**
1017 **PIN auxin efflux proteins during development.** SoPIN1 is in green, PIN1b in blue,
1018 and the putative partially functional *pin1-4* protein is in grey. Red arrows indicate
1019 measured auxin transport in the basal internode, while red bar-headed lines indicated
1020 reduced transport. Black lines represent polarized PIN patterns. Convergence points
1021 are marked with asterisks. **(A)** When expressed in both the epidermis and internal
1022 tissues with *proAtPIN1* in wildtype Col-0, SoPIN1 forms convergent polarization
1023 patterns in the epidermis and is partially able to rescue the organ initiation phenotypes
1024 and bulk transport in null *pin1-613* mutants. **(B)** When SoPIN1 is expressed only in
1025 the epidermis from the *proAtML1* promoter, it forms convergence points in the wild
1026 type background and is able to rescue more fully the organ initiation phenotypes of
1027 the *pin1-4* single amino acid change mutation in *Ler*. **(C)** In contrast, when PIN1b is
1028 expressed in both the epidermis and internal tissues from the *proAtPIN1* promoter in
1029 wildtype Col-0, it accumulates mostly in the internal tissues, and is unable to
1030 complement the *pin1-613* organ initiation phenotype. It is also unable to transport
1031 auxin through stem segments, despite apparently AtPIN1-like accumulation and
1032 polarization in the stem. **(D)** When PIN1b is expressed in the epidermis from *proAtML1*
1033 promoter, it does not form convergent polarization patterns in the wildtype *Ler*
1034 background (blue ovals), but it does in the *pin1-4* background, where it is able to
1035 rescue the defective organ initiation phenotype and mediate bulk transport.
1036

1037 **Figure 7 - supplement 1. Brassicaceae-specific PIN1 domains.** **(A)** A wrapped
1038 protein alignment showing PIN1 clade members from across the angiosperms. Grass
1039 PIN1a proteins are indicated in grey, grass PIN1b proteins are indicated in black and
1040 Brassicaceae PIN1 proteins are indicated in red. Domains that are unique to the
1041 Brassicaceae family are indicated by transparent red boxes over the alignment. **(B)**
1042 Sequenced angiosperm species and version numbers, from
1043 <https://phytozome.jgi.doe.gov>. Species used in the alignment in **(A)** are indicated with
1044 green circles.

1045

1046 **Table 1. Oligos.** See methods for usage.

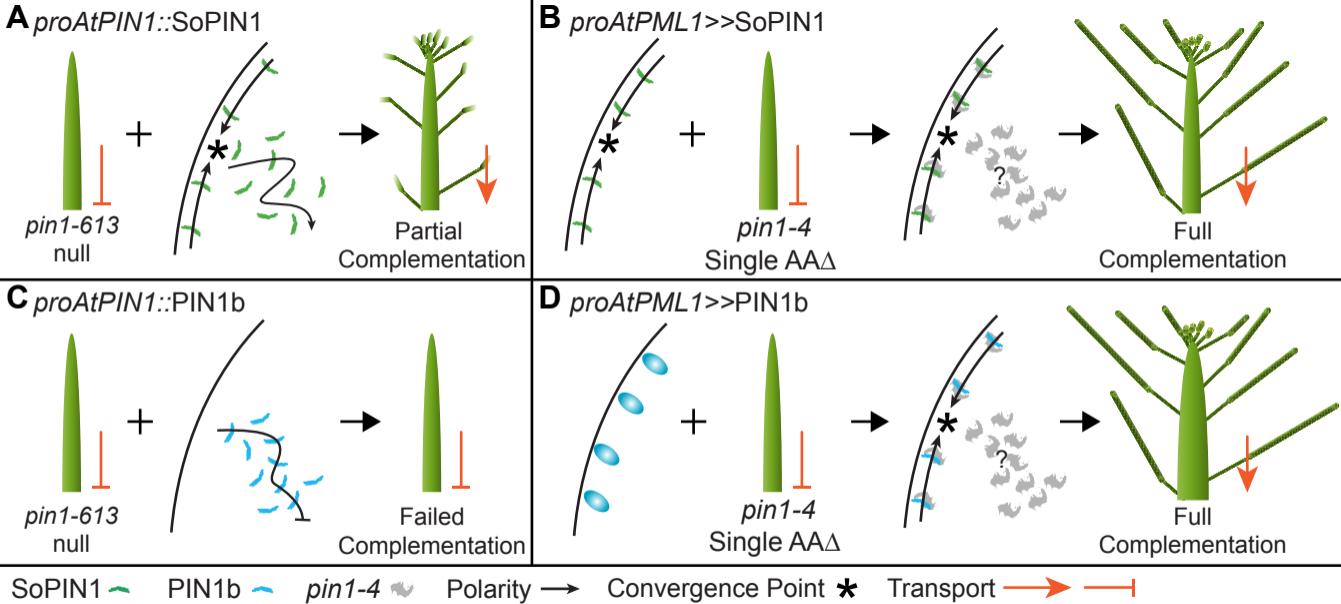


Figure 7

Table 1: Primers

ID#	Name	Sequence	Purpose
1	019 - Ubi-1 Prom attB4 F	GGGGACAACCTTTGTATAGAAAAGTTGCTGCAGTGCAGCGTGACCCGG	pZmUbi amplification for cloning
2	020 - Ubi-1 Prom attB1 R	GGGGACTGCTTTTTTTGTACAAACTTGCTGCAGAAGTAACACCAAACA	pZmUbi amplification for cloning
3	PIN1pro-GW-F	GGGGACAACCTTTGTATAGAAAAGTTGTTACCCTCATCCATCATTAACTT	<i>proAtPIN1</i> amplification
4	PIN1pro-GW-R	GGGGACTGCTTTTTTTGTACAAACTTGTCTTTTGTTCGCCGGAGAAGAGA	<i>proAtPIN1</i> amplification
5	455 BdSoPIN1 cacc mRNA	TCACATCTGCTGCCGCTGCC	SoPIN1-Citrine coding region amplification
6	302 - PIN_7 qPCR UTR R2	AATCCCAAAGCCGCACATTG	SoPIN1-Citrine coding region amplification
7	466 BdPIN1b cacc mRNA-2	CACCTGTACACACTGCGGCGCT	PIN1b-Citrine coding region amplification
8	308 - PIN_5 qPCR UTR R1	ACTCGCTAACCAACCCTTAATT	PIN1b-Citrine coding region amplification
9	MVR087 - pin1-613 RP (SALK_047613)	AATCATCACAGCCACTGATCC	<i>pin1-613</i> genotyping
10	MVR086 - pin1-613 LP (SALK_047613)	CAAAAACACCCCAAAATTC	<i>pin1-613</i> genotyping
11	MVR036 - LBb1.3	ATTTTGCCGATTCGGAAC	<i>pin1-613</i> genotyping
12	344 - Citrine Seq R	GAAGCACATCAGGCCGTAG	PIN1b-Citrine and SoPIN1-Citrine genotyping
13	524_Bradi4g26300_4230_F	CGTTCGGTGTGATCCGATG	SoPIN1-Citrine genotyping
14	541_Bradi3g59520_PIN1b_5084_F	TGATGCTCTTCATGTTCCGAGTACC	PIN1b-Citrine genotyping
15	543_pin1-4_Aci_F	GCTTTTGCGGCGGCTATGAGATTTGT	<i>pin1-4</i> genotyping
16	544_pin1-4_Aci_R	GCTTCTGATTTAATTTGTGGGTTTTCA	<i>pin1-4</i> genotyping
17	076 - BASTA_F2	CTTCAGCAGGTGGGTGTAGAG	ML1::LhG4 genotyping
18	077 - BASTA_R2	GAGACAAGCACGGTCAACTTC	ML1::LhG4 genotyping